Lecture notes for

Mathematical Cell Biology

Christian Schmeiser[1]

Contents

[1]Fakultät für Mathematik, Universität Wien, Oskar-Morgenstern-Platz 1, 1090 Wien, Austria. christian.schmeiser@univie.ac.at

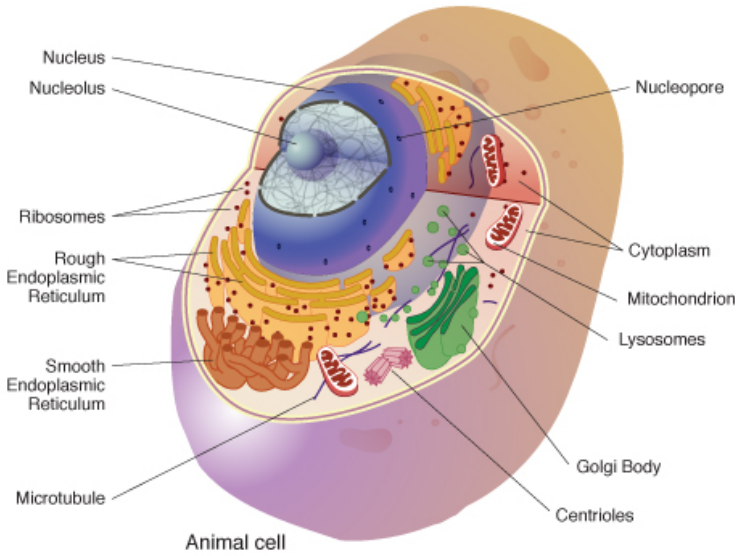

Figure 1: Some of the most important organelles of animal cells. Source: `wikipedia`

1 Introduction

The cell could serve as the basis for a definition of life on earth, at least from a practical if not from a philosophical point of view. It is often called the *basic unit of life,* since it is a building block of all living beings. Considering the enormous variety of life on earth, it is by no means obvious that it makes sense to talk about *the* cell. This can be motivated by the astonishing fact that all different cell types share a number of basic properties hinting to a very small number of common ancestors. For these reasons, cell biology is not just an ever growing collection of (unrelated) facts about cells, but a scientific field with a large common basis and with systematic approaches to extending our knowledge. Cell biology explains the structure and organization of cells, their physiological properties, metabolic processes, signaling pathways, life cycle, and interactions with their environment. Knowing the components of cells and how cells work is fundamental to all biological sciences.

The strongly related field *molecular biology* concentrates on detailed chemical aspects. Biochemistry is characterized by the occurrence of only a small number of elements, which are however combined into sometimes

very large molecules. The 4 most common elements *carbon (C), hydrogen (H), nitrogen (N),* and *oxygen (O)* make up for about 96.5% of the mass of a cell, with the rest provided mostly by the less common elements *calcium (Ca), chlorine (Cl), magnesium (Mg), phosphorus (P), potassium (K), sodium (Na),* and *sulfur (S).* The molecules in cells are mainly water (appr. 85%), lipids (fat molecules), and proteins (large molecules responsible for all cell activities). The information about the cell identity is stored in the desoxyribonucleic acid (DNA). Parts of this information are distributed and used in the cell via ribonucleic acids (RNA).

Cells are divided into two main categories: *prokaryotes* and *eukaryotes.* The main difference is that prokaryotes do not have a nucleus and a much simpler internal organisation. This category contains archaea and bacteria, both unicellular organisms, whereas eukaryotic cells occur in animals, plants, fungi, and protista (or protozoa). Animals, plants, and fungi are multicellular with sometimes huge numbers of cells per individual (3.72×10^{13} for the average human adult, according to an estimate published in 2013 [2]). Cell biology focuses more on the study of eukaryotic cells than on prokaryotes, which are covered in the field of *microbiology.* Eukaryotic cells have separated compartments called *organelles,* serving well defined functions. In the following we list some of them (see also Fig. 1):

Centrosome: an associated pair of cylindrical shaped protein structures (centrioles) that organize microtubules.

Cell membrane (plasma membrane): the part of the cell which separates the cell from the outside environment as well as cellular compartments from each other. It also contributes to the regulation of cellular processes.

Cell wall: extra layer of protection and gives structural support (only found in plant cells).

Chloroplast: key organelle for photosynthesis (only found in plant cells).

Cytoplasm: contents of the main fluid-filled space inside cells, where many chemical reactions happen.

Cytoskeleton: protein filaments inside cells (microfilaments, microtubules, and intermediate filaments), serves several functions, such as cell shape changes, cell movement, intracellular transportation and signaling.

Endoplasmic reticulum (rough): major site of membrane protein synthesis.

Endoplasmic reticulum (smooth): major site of lipid synthesis.

Golgi apparatus: distribution system for proteins.

Lysosome: acidic organelle that breaks down cellular waste products and debris into simple compounds (only found in animal cells).

Mitochondrion: power plant of the cell, storing energy in Adenosin triphosphate (ATP).

Nucleus: contains chromosomes composed of DNA

Ribosome: RNA and protein complex required for protein synthesis in cells

Vesicle: small membrane-bounded spheres inside cells

Theoretical cell biology tries to explain cellular mechanisms in terms of *chemical* and/or *mechanical* processes. It typically suffices to use a standard stochastic description of chemical reactions and classical (i.e. Newtonian) mechanics. Such explanations can be formulated in terms of mathematical models. The formulation of these models, their solution, and the biological interpretation of model properties make up the field of *mathematical cell biology,* the subject of this course, which covers only a small section of this rapidly growing field.

2 Mathematical models for chemical reactions

2.1 Models for mass-action kinetics

Chemical substances might be very unevenly distributed in cells with strong effects on reactions between them. For simplicity we shall start, however, assuming a *well mixed reactor,* where it suffices to describe the substances $X_1, \ldots, X_n$ by their *concentrations* $c(t) = (c_1(t), \ldots, c_n(t))$ at time t, measured in numbers of molecules per volume.

The concentrations change with time as the consequence of m chemical reactions with the *reaction rates* $r(t) = (r_1(t), \ldots, r_m(t))$ and the *stoichiometric coefficients* $\nu_{ij} \in \mathbb{Z}$, $i = 1, \ldots, n$, $j = 1, \ldots, m$. The reaction rates describe, how many times per volume and per time a reaction takes place. The stoichiometric coefficients describe the book keeping: When $\nu_{ij} > 0$, each occurrence of reaction number j produces ν_{ij} molecules of the substance X_i. Whereas for $\nu_{ij} < 0$ each occurrence of reaction number j destroys $-\nu_{ij}$

molecules of the substance X_i. For $\nu_{ij} = 0$ the substance X_i is not involved in reaction number j. The *stoichiometric matrix* is given by

$$N = \begin{pmatrix} \nu_{11} & \cdots & \nu_{1m} \\ \vdots & & \vdots \\ \nu_{n1} & \cdots & \nu_{nm} \end{pmatrix} .$$

The model for the evolution of the concentrations is the ODE system

$$\frac{dc}{dt} = Nr \, .$$

For so called *simple reactions,* the reaction rates can be modeled by the *mass action law*

$$r_j = k_j \prod_{i:\, \nu_{ij}<0} c_i^{-\nu_{ij}} \, , \qquad j = 1, \ldots, m \, ,$$

with the *reaction constants* $k_j > 0$. The product contains a factor c_i for each molecule of X_i entering the reaction. The total number

$$- \sum_{i:\, \nu_{ij}<0} \nu_{ij}$$

of these molecules is called the *order of the reaction.* For given reaction constants and stoichiometric coefficients, the concentrations can be computed, when also initial conditions

$$c_i(0) = c_{i0} \, , \qquad i = 1, \ldots, n \, ,$$

for the concentrations are prescribed. Since we have assumed time independence of the data, the choice $t = 0$ for the initial time does not mean a loss of generality.

A simple example: Let us consider the reaction $X_1 + X_2 \to X_3$ and its reverse with the stoichiometric matrix

$$N = \begin{pmatrix} -1 & 1 \\ -1 & 1 \\ 1 & -1 \end{pmatrix} .$$

Thus, we have the rates $r_+ = k_+ c_1 c_2$ for the second order forward reaction and $r_- = k_- c_3$ for the first order reverse reaction, leading to the ODEs

$$\frac{dc_1}{dt} = k_- c_3 - k_+ c_1 c_2 \, , \quad \frac{dc_2}{dt} = k_- c_3 - k_+ c_1 c_2 \, , \quad \frac{dc_3}{dt} = k_+ c_1 c_2 - k_- c_3 \, ,$$

subject to initial conditions

$$c_1(0) = c_{10}\,, \quad c_2(0) = c_{20}\,, \quad c_3(0) = c_{30}\,.$$

We can use the *conservation laws*

$$\frac{dc_1}{dt} - \frac{dc_2}{dt} = 0 \quad \text{and} \quad \frac{dc_1}{dt} + \frac{dc_3}{dt} = 0\,,$$

and their consequence

$$c_2(t) = c_1(t) - c_{10} + c_{20}\,, \qquad c_3(t) = -c_1(t) + c_{10} + c_{30}\,,$$

to reduce the system to the scalar equation

$$\frac{dc_1}{dt} = f(c_1)\,, \quad \text{mit } f(c_1) = k_-(c_{10} + c_{30}) - c_1(k_- + k_+c_{20} - k_+c_{10}) - k_+c_1^2\,,$$

which possesses a unique, positive, asymptotically stable equilibrium.

A zeroth order reaction: Now we consider $X_1 \to X_2$ and the reverse reaction (both first order), leading to the initial value problem

$$\frac{dc_1}{dt} = k_-c_2 - k_+c_1\,, \quad \frac{dc_2}{dt} = k_+c_1 - k_-c_2\,, \qquad c_1(0) = c_{10}\,, \quad c_2(0) = c_{20}\,.$$

We assume that the reverse reaction has a much smaller reaction constant, i.e. $k_- \ll k_+$. The reaction rates can only be of the same order of magnitude, if c_1 is much smaller than c_2, which we assume for their initial values: $c_{10} \ll c_{20}$. We shall analyse the consequences of these assumptions by an appropriate *scaling*. In particular, we shall use *intrinsic reference quantities,* i.e. units for the variables computed from the parameters of the problem.

We choose the initial values for the concentrations and $1/k_+$ for time. This means to introduce the transformations

$$u_1(\tau) = \frac{c_1(\tau/k_+)}{c_{10}}\,, \qquad u_2(\tau) = \frac{c_2(\tau/k_+)}{c_{20}}\,,$$

where u_1, u_2, and τ are the dimensionless quantities. This leads to

$$u_1' = \frac{u_2}{a} - u_1\,, \quad u_2' = \varepsilon(au_1 - u_2)\,, \qquad u_1(0) = u_2(0) = 1\,, \tag{1}$$

with the dimensionless parameters $\varepsilon \ll 1$ and a (assumed of moderate size), defined by

$$\frac{k_-}{k_+} = \varepsilon\,, \qquad \frac{c_{10}}{c_{20}} = \varepsilon a\,.$$

The limit $\varepsilon \to 0$ gives the approximation $u_2(\tau) = 1$ for $\tau \geq 0$ and

$$u_1' = \frac{1}{a} - u_1\,, \qquad u_1(0) = 1\,.$$

The rate of the reverse reaction is approximated by $1/a$, which is called a *zeroth order reaction.* The substance X_2 is taken from a big reservoir, approximately uneffected by the reaction.

2.2 Michaelis-Menten-Kinetics

Assume the enzyme E controls a reaction, where the substrate S is transformed to the product P. This happens in two partial reactions, where enzyme and substrate first build the complex ES, which is then decomposed into the product and the unchanged enzyme, i.e. $E + S \to ES \to P + E$. We assume that initially there is only enzyme and substrate with a much smaller enzyme concentration. This leads to the initial value problem

$$\begin{aligned} c_S' &= -k_1 c_E c_S\,, \qquad c_S(0) = c_{S0}\,, \\ c_E' &= k_2 c_{ES} - k_1 c_E c_S\,, \qquad c_E(0) = c_{E0}\,, \\ c_{ES}' &= k_1 c_E c_S - k_2 c_{ES}\,, \qquad c_{ES}(0) = 0\,, \\ c_P' &= k_2 c_{ES}\,, \qquad c_P(0) = 0\,. \end{aligned}$$

We introduce the scaling $u_S = c_S/c_{S0}$, $u_P = c_P/c_{S0}$, $u_E = c_E/c_{E0}$, $u_{ES} = c_{ES}/c_{E0}$, and $\tau = k_1 c_{E0} t$:

$$\begin{aligned} u_S' &= -u_E u_S\,, \qquad u_S(0) = 1\,, \\ \varepsilon\, u_E' &= a\, u_{ES} - u_E u_S\,, \qquad u_E(0) = 1\,, \\ \varepsilon\, u_{ES}' &= u_E u_S - a\, u_{ES}\,, \qquad u_{ES}(0) = 0\,, \\ u_P' &= a\, u_{ES}\,, \qquad u_P(0) = 0\,, \end{aligned} \tag{2}$$

with the dimensionless parameters

$$\varepsilon = \frac{c_{E0}}{c_{S0}} \ll 1\,, \qquad a = \frac{k_2}{k_1 c_{S0}}\,.$$

Adding the second and the third differential equation gives the conservation law

$$u_E(\tau) + u_{ES}(\tau) = 1\,.$$

This and the limit $\varepsilon \to 0$ in the second equation lead to $0 = a(1-u_E) - u_E u_S$ and, thus,

$$u_E(\tau) = \frac{a}{a + u_S(\tau)}\,. \tag{3}$$

The result is a direct reaction rate for $S \to P$:

$$u'_P = -u'_S = \frac{a\, u_S}{a + u_S}\,,$$

or, in terms of the original unscaled variables,

$$c'_P = -c'_S = \frac{k_1 k_2 c_{E0} c_S}{k_2 + k_1 c_S}\,.$$

This result is called *Michaelis-Menten kinetics* [11]. It can be seen as an interpolation between a first order reaction (rate $\approx k_1 c_{E0} c_S$) for small values of c_S and a zeroth order reaction (rate $\approx k_2 c_{E0}$) for large values of c_S.

The system (4) is called *singularly perturbed,* as opposed to the *regularly perturbed* system (1), because two of the differential equations become algebraic equations in the limit $\varepsilon \to 0$. Note that in the limit, the approximations for the *fast variables* $u_E = a/(a+u_S)$ and $u_{ES} = u_S/(a+u_S)$ cannot satisfy the correct initial conditions, whereas the initial values for the approximations of the *slow variables* u_S and u_P can be chosen appropriately. The solution to this dilemma is to consider the *fast time scale* $\sigma = \tau/\varepsilon$. In terms of this new variable, the problem takes the regularly perturbed form

$$\begin{aligned}
\frac{du_S}{d\sigma} &= -\varepsilon u_E u_S\,, \qquad u_S(0) = 1\,,\\
\frac{du_E}{d\sigma} &= a\, u_{ES} - u_E u_S\,, \qquad u_E(0) = 1\,,\\
\frac{du_{ES}}{d\sigma} &= u_E u_S - a\, u_{ES}\,, \qquad u_{ES}(0) = 0\,,\\
\frac{du_P}{d\sigma} &= \varepsilon a\, u_{ES}\,, \qquad u_P(0) = 0\,,
\end{aligned} \tag{4}$$

The limit $\varepsilon \to 0$ now leads to the *initial layer approximation*

$$u_E = \frac{a + e^{-\sigma(1+a)}}{a+1}\,, \tag{5}$$

whose limit $a/(a+1)$ as $\sigma \to \infty$ coincides with the value of the approximation (3) for $\tau = 0$, a *matching relation* in the language of singular perturbation theory.

2.3 First order weakly reversible systems

We consider reaction networks with only first order reactions of the form $X_i \to X_j$ with reaction constant $k_{ij} \geq 0$, $i, j = 1, \ldots, n$, $i \neq j$. It is useful to

represent the network as a directed graph with nodes X_i, $i = 1, \ldots, n$, and an edge directed from X_i to X_j, iff $k_{ij} > 0$. The ODE system modeling the network is

$$\frac{dc_i}{dt} = \sum_{j \neq i} (k_{ji} c_j - k_{ij} c_i) \,, \qquad i = 1, \ldots, n, \tag{6}$$

with initial condition $c_i(0) = c_{i,0} \geq 0$, $i = 1, \ldots, n$. Since, obviously,

$$\sum_{i=1}^{n} \frac{dc_i}{dt} = 0 \,,$$

the total number of molecules is conserved:

$$\sum_{i=1}^{n} c_i(t) = \sum_{i=1}^{n} c_{i,0} =: M \,, \qquad t \geq 0 \,.$$

It is also easily seen that $c_i(t) \geq 0$ for $i = 1, \ldots, n$, $t \geq 0$ is a consequence of the nonnegativity of the initial data. The dynamics is therefore restricted to a compact subset of a hyperplane.

We pose the question of the existence of a *positive equilibrium* $(c_{1,\infty}, \ldots, c_{n,\infty})$, where *positive* means that all concentrations are positive: $c_{i,\infty} > 0$, $i = 1, \ldots, n$. Considering for a moment the case $n = 2$ shows that we need either $k_{12}, k_{21} > 0$ or the trivial case $k_{12} = k_{21} = 0$. For $n > 2$ the situation is more complicated.

Definition 1 *A directed graph is* weakly reversible*, iff for every edge $X_i \to X_j$ it contains a path $X_j \to X_{i_1} \to \ldots \to X_{i_r} \to X_i$.*

Lemma 1 *Let the directed graph corresponding to (6) be connected and weakly reversible, and let $M > 0$. Then there exists a unique positive equilibrium with total concentration M, i.e. there exists $(c_{1,\infty}, \ldots, c_{n,\infty})$ with*

$$\begin{aligned} &\sum_{j \neq i} (k_{ji} c_{j,\infty} - k_{ij} c_{i,\infty}) = 0 \,, \quad c_{i,\infty} > 0 \,, \qquad i = 1, \ldots, n \,, \\ &\sum_{i=1}^{n} c_{i,\infty} = M \,. \end{aligned} \tag{7}$$

For a proof see [4]. We claim that, in the situation of the Lemma,

$$L(t) := \frac{1}{2} \sum_{i=1}^{n} c_{i,\infty} u_i(t)^2 \,, \qquad \text{with } u_i(t) := \frac{c_i(t) - c_{i,\infty}}{c_{i,\infty}} \tag{8}$$

is a Lyapunov function:

$$\begin{aligned}\frac{dL}{dt} &= \sum_{i=1}^{n}\sum_{j\neq i} u_i(k_{ji}c_j - k_{ij}c_i) = \sum_{i=1}^{n}\sum_{j\neq i} u_i\left(k_{ji}(c_j - c_{j,\infty}) - k_{ij}(c_i - c_{i,\infty})\right) \\ &= \sum_{i=1}^{n}\sum_{j\neq i} u_i\left(k_{ji}c_{j,\infty}u_j - k_{ij}c_{i,\infty}u_i\right)\,,\end{aligned}$$

where, for the second equality, we have used the equilibrium property (7). For the second term, we derive two different representations:

$$\begin{aligned}\sum_{i=1}^{n}\sum_{j\neq i} k_{ij}c_{i,\infty}u_i^2 &= \sum_{j\neq i} k_{ji}c_{j,\infty}u_j^2 \qquad \text{and} \\ \sum_{i=1}^{n}\sum_{j\neq i} k_{ij}c_{i,\infty}u_i^2 &= \sum_{j\neq i} k_{ji}c_{j,\infty}u_i^2\,,\end{aligned}$$

where the first follows from $i \leftrightarrow j$ and the second again from (7). Using half of each of these, we get

$$\begin{aligned}\frac{dL}{dt} &= \sum_{i=1}^{n}\sum_{j\neq i} k_{ji}c_{j,\infty}\left(u_iu_j - \frac{1}{2}u_i^2 - \frac{1}{2}u_j^2\right)\,, \\ &= -\frac{1}{2}\sum_{i=1}^{n}\sum_{j\neq i} k_{ji}c_{j,\infty}\left(u_i - u_j\right)^2 \leq 0\,.\end{aligned}$$

Not only is L a Lyapunov function, but under the assumptions already made, the right hand side above can be shown to be negative definite.

Lemma 2 *Under the assumptions of Lemma 1 there exists $\gamma > 0$ such that*

$$\sum_{i=1}^{n}\sum_{j\neq i} k_{ji}c_{j,\infty}\left(u_i - u_j\right)^2 \geq \gamma\sum_{i=1}^{n} c_{i,\infty}u_i^2\,,$$

holds for all $(u_1, \ldots, u_n) \in \mathbb{R}^n$ such that $\sum_i c_{i,\infty}u_i = 0$.

A proof can again be found in [4]. Since the condition at the end of the lemma is satisfied because of (8), this implies the differential inequality

$$dL/dt \leq -\gamma L\,, \tag{9}$$

and, with the Gronwall lemma (see below),

$$L(t) \leq e^{-\gamma t}L(0)\,.$$

Theorem 1 *Under the assumptions of Lemma 1 there exist $\alpha, \gamma > 0$ such that*

$$|c_i(t) - c_{i,\infty}| \le \alpha e^{-\gamma t/2}\,, \qquad i = 1, \dots, n\,.$$

Concerning the Gronwall lemma, we first state that (9) implies

$$L(t) \le L(\tau) - \gamma \int_\tau^t L(s)ds\,, \qquad 0 \le \tau \le t\,. \tag{10}$$

Lemma 3 (Gronwall, decaying) *Let $L \in C([0,\infty))$ satisfy $L(t) \ge 0$ and (10) with $\gamma \ge 0$. Then*

$$L(t) \le e^{-\gamma t} L(0)\,, \qquad t \ge 0\,.$$

Proof: Assume there exists $t^* > 0$, such that $L(t^*) > e^{-\gamma t^*} L(0) =: \overline{L}(t^*)$. Let

$$\hat{t} := \max\{t \in [0, t^*) : \, L(t) = \overline{L}(t)\}\,,$$

i.e. $L(\hat{t}) = \overline{L}(\hat{t})$ and

$$L > \overline{L} \qquad \text{in } (\hat{t}, t^*]\,. \tag{11}$$

We also define

$$\varphi(t) = L(\hat{t}) - \gamma \int_{\hat{t}}^t L(s)ds\,.$$

Then $\varphi(\hat{t}) = \overline{L}(\hat{t})$ and

$$\frac{d}{dt}(\varphi/\overline{L}) = \frac{\gamma(\varphi - L)}{\overline{L}} \ge 0$$

by (10). This implies $\varphi \ge \overline{L}$ in $[\hat{t}, t^*]$, which is equivalent to

$$\int_{\hat{t}}^t L(s)ds \le \int_{\hat{t}}^t \overline{L}(s)ds\,, \qquad t \in [\hat{t}, t^*]\,.$$

This is a contradiction to (11). ∎

The above result is an extension [15] of the classical Gronwall lemma (in integral form) for exponentially growing bounds, which needs a weaker assumption and is easier to prove:

Lemma 4 (Gronwall, growing) *Let $L \in C([0,\infty))$ satisfy $L(t) \ge 0$ and $L(t) \le L(0) + \gamma \int_0^t L(s)ds$, $t \ge 0$, with $\gamma \ge 0$. Then*

$$L(t) \le e^{\gamma t} L(0)\,, \qquad t \ge 0\,.$$

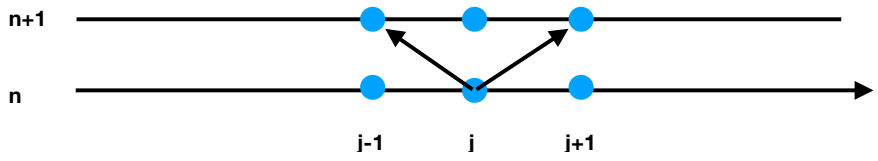

Figure 2: Jump process on a one-dimensional grid

Proof: The function

$$v(t) := e^{-\gamma t} \int_0^t L(s) ds$$

satisfies

$$\frac{dv}{dt}(t) = e^{-\gamma t} \left(L(t) - \gamma \int_0^t L(s) ds \right) \leq e^{-\gamma t} L(0) \, .$$

By integration we obtain

$$v(t) \leq \frac{L(0)}{\gamma} \left(1 - e^{-\gamma t} \right) \, .$$

Since $L(t) \leq L(0) + \gamma e^{\gamma t} v(t)$, the result follows. Note that $\gamma \geq 0$ is used in this last step. ∎

3 Random motion of atoms and molecules

Atoms and molecules in cells live in a complex nonhomogeneous environment influencing their movement. As a consequence, for an observer this movement looks like having a random component. We therefore accept a random nature of this movement as a postulate for a mathematical description.

We start by approximating this movement by a jump process on a grid, and we first restrict to one spatial dimension for simplicity. Let $x_j = j\Delta x$, $j \in \mathbb{Z}$, denote the possible positions of particles, and assume that at the discrete points $t_n = n\Delta t$, $n \in \mathbb{Z}$, in time particles perform jumps of the length Δx to the left or to the right (see Fig. 2). Let us assume further that the probability of jumping to the left is q, and the probability of jumping to the right is $1 - q$ (with $0 \leq q \leq 1$, of course). Now we introduce the nonnegative quantities p_j^n, $j, n \in \mathbb{Z}$, which can be interpreted either as the probability that one particle is at the position x_j at time t_n or as the

expected number of particles out of a large ensemble at position x_j at time t_n or (if the latter is divided by Δx) as the expected number density of particles at position x_j at time t_n. Then, obviously the values at time t_{n+1} can be computed in terms of the values at time t_n:

$$p_j^{n+1} = qp_{j+1}^n + (1-q)p_{j-1}^n \tag{12}$$

Eventually we are looking for continuous descriptions both in time and in position. Therefore we shall interpret p_j^n as approximation for $p(x_j, t_n)$ where p is a function of two real valued arguments. With this interpretation in mind we rewrite the above equation as

$$p_j^{n+1} - p_j^n = q(p_{j+1}^n - p_j^n) - (1-q)(p_j^n - p_{j-1}^n)\,,$$

and further,

$$\frac{p_j^{n+1} - p_j^n}{\Delta t} - \frac{q\Delta x}{\Delta t}\,\frac{p_{j+1}^n - p_j^n}{\Delta x} + \frac{(1-q)\Delta x}{\Delta t}\,\frac{p_j^n - p_{j-1}^n}{\Delta x} = 0\,.$$

Our aim is to pass to the limit $\Delta x, \Delta t \to 0$. Obviously the result depends on the relative size of Δx and Δt. We have three main options: Either the grid speed $s := \Delta x/\Delta t$ tends to zero, to infinity, or we keep it fixed at a positive finite value. The most interesting result occurs in the latter case, which we call the *significant limit*:

$$\partial_t p + \partial_x(vp) = 0\,, \qquad \text{with } v = s(1-2q)\,. \tag{13}$$

Actually, the other two cases can be recovered by letting $s \to 0$ or $s \to \infty$.

Equation (13) is a one-dimensional *convection equation*. Solutions are travelling waves $p(x,t) = f(x - vt)$ with velocity v. With the interpretation of p as time dependent density of particles along the line, the integrated version of (13),

$$\frac{d}{dt}\int_a^b p(x,t)dx + vp(b,t) - vp(a,t) = 0\,,$$

gives the rate of change of the number of particles contained in the interval (a,b). The term $j(x,t) = vp(x,t)$ can then be interpreted as the *flux* of particles through the point x at time t, and v is the mean velocity of particles. Any partial differential equation of the form

$$\partial_t p + \partial_x j = 0\,, \tag{14}$$

can be interpreted as a *one-dimensional conservation law* with density p and flux j.

It is interesting to note that equation (13) could have been derived without any probabilistic effects. The assumption that all particles always move to the right or always to the left, i.e., $q = 0$ or $q = 1$, still leads to (13) with $v = \pm s$. More generally, the same value of v, and therefore the same macroscopic equation (13) can be obtained by different choices of the grid speed s and of the probability q. This shows that the properties of the microscopic movement cannot be completely recovered from macroscopic observations.

In the symmetric situation $q = 1/2$, the mean velocity vanishes, and (13) becomes trivial. This unsatisfactory situation can be clarified by returning to the discrete equation (12) and by rewriting it in a different way:

$$\frac{p_j^{n+1} - p_j^n}{\Delta t} - \frac{(\Delta x)^2}{2\Delta t} \frac{p_{j+1}^n - 2p_j^n + p_{j-1}^n}{(\Delta x)^2} = 0\,.$$

This shows that for $q = 1/2$, the significant limit is achieved, when $D = (\Delta x)^2/(2\Delta t)$ is kept fixed as $\Delta x, \Delta t \to 0$:

$$\partial_t p - D\partial_x^2 p = 0\,. \tag{15}$$

This is the one-dimensional *diffusion equation* with diffusivity D. Integration as above shows that the diffusive flux is given by *Fick's law*

$$j = -D\partial_x p\,. \tag{16}$$

So far we have seen that the macroscopic limit of a biased random motion is a convection equation, and for an unbiased motion it is a diffusion equation. Actually, both effects can be combined in the macroscopic equation by an appropriate scaling assumption. We shall also generalize the position jump process by allowing a dependence of the jump probability on position and time:

$$p_j^{n+1} = q_{j+1}^n p_{j+1}^n + (1 - q_{j-1}^n) p_{j-1}^n\,.$$

As in the derivation of the diffusion equation we assume that $D = (\Delta x)^2/(2\Delta t)$ is fixed and that the jump probabilities are close to $1/2$:

$$q_j^n = \frac{1}{2} - \frac{v(x_j, t_n)\Delta t}{2\Delta x} = \frac{1}{2} - \frac{v(x_j, t_n)}{4D}\Delta x\,,$$

where $v(x, t)$ is a given velocity function. Using this we obtain

$$p_j^{n+1} = \frac{p_{j+1}^n + p_{j-1}^n}{2} - \frac{\Delta t}{2\Delta x}(v_{j+1}^n p_{j+1}^n - v_{j-1}^n p_{j-1}^n)\,,$$

and, subtracting p_j^n and dividing by Δt,

$$\frac{p_j^{n+1} - p_j^n}{\Delta t} = D\frac{p_{j+1}^n - 2p_j^n + p_{j-1}^n}{\Delta x^2} - \frac{1}{2\Delta x}(v_{j+1}^n p_{j+1}^n - v_j^n p_j^n + v_j^n p_j^n - v_{j-1}^n p_{j-1}^n)\,,$$

The limits $\Delta t, \Delta x \to 0$ now lead to the one-dimensional *convection-diffusion equation*

$$\partial_t p + \partial_x(vp - D\partial_x p) = 0\,. \tag{17}$$

Everything we did so far can be extended to higher dimensions with the result

$$\partial_t p + \nabla \cdot (vp - D\nabla p) = 0\,, \tag{18}$$

where now the density $p(x,t)$ depends on position $x \in \mathbb{R}^d$, with $d = 2$ or $d = 3$, and on time $t \in \mathbb{R}$. The gradient with respect to x is denoted by ∇ and the divergence by $\nabla\cdot$. The velocity $v(x,t)$ and the flux $vp - D\nabla p$ are vector fields. The interpretation of the flux vector is the following: Its component in the direction ν is the number of particles per time and per unit area moving through an area element orthogonal to ν. This can be seen by integrating (18) over a bounded position domain $\Omega \subset \mathbb{R}^d$ and using the divergence theorem:

$$\frac{d}{dt}\int_\Omega p\,dx + \int_{\partial\Omega}(vp - D\nabla p)\cdot\nu\,d\sigma = 0\,, \tag{19}$$

where ν denotes the unit outward normal vector along the boundary $\partial\Omega$, and $d\sigma$ is the line element for $d = 2$ and the surface element for $d = 3$.

Remark 1 *Note that for the diffusion rotational symmetry holds, i.e. the Laplace operator is not changed under a rotation of the coordinate system. This might seem rather surprising, when it is derived from the dynamics on a rectangular grid, which obviously has preferred directions.*

So far we have only described the movement of particles. Equation (18) is a conservation law. No particles are created or destroyed. As the final step in this modelling section, we also allow for this possibility. We denote by $f(x,t)$ the number of particles created or destroyed (depending on the sign of f) per unit time and unit volume. Then the right hand side of (19) has to be replaced by the integral of f over Ω, and the differential version (18) becomes the *reaction-convection-diffusion equation*

$$\partial_t p + \nabla \cdot (vp - D\nabla p) = f\,. \tag{20}$$

Why reaction? In a typical situation our particles are molecules whose creation or destruction is the result of a chemical reaction.

In the following, systems of equations of the form (20) for different species of particles will be considered, when x varies in a domain $\Omega \subset \mathbb{R}^d$, representing the whole cell or a cell compartment. Typically we shall use zero flux boundary conditions

$$(vp - D\nabla p) \cdot \nu = 0 \quad \text{along } \partial\Omega\,.$$

For given v and f, the formulation of a well posed problem for the unknown p is completed by prescribing initial conditions $p(x,0) = p_I(x)$ for $x \in \Omega$, with given initial data p_I. Well posedness means that the initial-boundary value problem has a unique solution continuously dependent (in an appropriate sense) on the data v, f, and p_I.

4 Gene regulatory networks

4.1 Transcription and translation

The main source for the material of this section is [1].

DNA can be subdivided into *genes,* each of which contains a code identifying a protein. The subject of this section is *gene expression,* which is (not exclusively, but mostly) the process of the production of these proteins. From an information point of view, a gene can be interpreted as a word written in a 4-letter-alphabet, where the letters are called *adenine, cytosine, guanine,* and *thymine.* Similarly a protein can be seen as a word, however written in a 20-letter-alphabet with *amino acids* as letters. So how are genes translated into proteins? It is an amazing fact that the answer is almost universal for all living species. It is called the *genetic code.* Each group of three letters of the gene, called a *codon,* uniquely determines an amino acid (see Fig. 3). Since there are $4^3 = 64$ different codons, there is a lot of redundancy in the sense that several codons code for the same amino acid.

It is an obvious fact that each cell has to make decisions about how much of each protein is produced at each time. For example, in multicellular organisms this determines the cell type. *Gene regulation* is the name for the mechanisms for making these decisions. It determines the map from the *genotype* (i.e. the DNA) to the *phenotype* (i.e. observable traits and functionality of the cell).

The production of a protein typically requires two steps:

Amino acid	DNA codons	Compressed	Amino acid	DNA codons	Compressed
Ala / A	GCT, GCC, GCA, GCG	GCN	Ile / I	ATT, ATC, ATA	ATH
Arg / R	CGT, CGC, CGA, CGG; AGA, AGG	CGN, AGR; or CGY, MGR	Leu / L	CTT, CTC, CTA, CTG; TTA, TTG	CTN, TTR; or CTY, YTR
Asn / N	AAT, AAC	AAY	Lys / K	AAA, AAG	AAR
Asp / D	GAT, GAC	GAY	Met / M	ATG	
Asn or Asp / B	AAT, AAC; GAT, GAC	RAY	Phe / F	TTT, TTC	TTY
Cys / C	TGT, TGC	TGY	Pro / P	CCT, CCC, CCA, CCG	CCN
Gln / Q	CAA, CAG	CAR	Ser / S	TCT, TCC, TCA, TCG; AGT, AGC	TCN, AGY
Glu / E	GAA, GAG	GAR	Thr / T	ACT, ACC, ACA, ACG	ACN
Gln or Glu / Z	CAA, CAG; GAA, GAG	SAR	Trp / W	TGG	
Gly / G	GGT, GGC, GGA, GGG	GGN	Tyr / Y	TAT, TAC	TAY
His / H	CAT, CAC	CAY	Val / V	GTT, GTC, GTA, GTG	GTN
START	ATG		STOP	TAA, TGA, TAG	TRA, TAG

Figure 3: The genetic code. Source: `wikipedia`

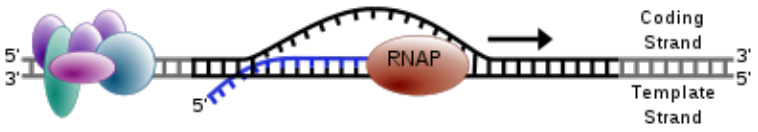

Figure 4: The process of transcription is carried out by RNA polymerase (RNAP), which uses DNA (black) as a template and produces RNA (blue). Source: `wikipedia`

- **Transcription** is the process, where a copy of the gene, called *messenger RNA (mRNA)* is produced (see Fig. 4).
- **Translation** is the actual production of the protein in a *ribosome,* a molecular machine, using the mRNA as input (see Fig. 5).

Very often (but not exclusively) gene regulation affects the transcription process. Typically a molecule binds to a so called *promotor site* of a gene either up- or down-regulating transcription. Accordingly, the molecule is called an *activator* or, respectively, a *repressor.* As a first step in the mathematical modelling, we describe the binding and unbinding of activators and repressors, reactions of the form $F + mA \to B$, where m molecules of type A bind to a free promotor site F, producing a bound promotor site B, and the reverse reaction. Considering the molecule concentration $c_A(t)$ as given,

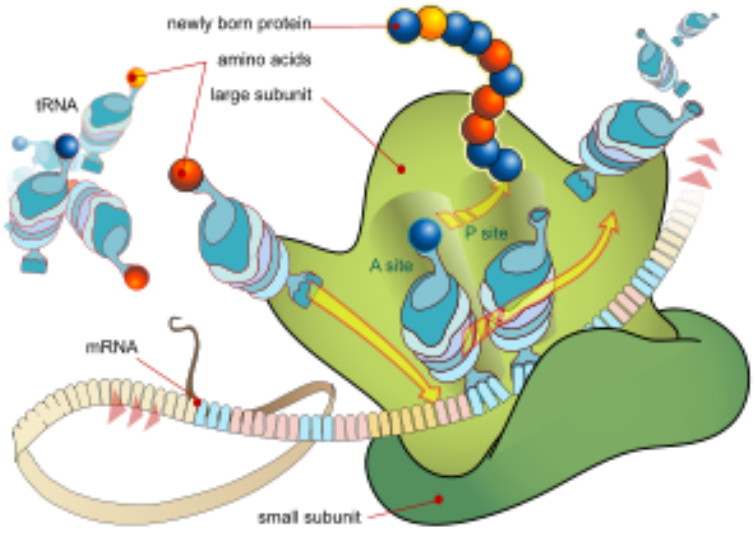

Figure 5: During the translation, tRNA charged with amino acid enters the ribosome and aligns with the correct mRNA triplet. Ribosome then adds amino acid to growing protein chain. Source: `wikipedia`

the rules of Section 2 imply

$$\frac{dc_B}{dt} = -\frac{dc_F}{dt} = k_1 c_F c_A^m - k_2 c_B \,.$$

Assuming this process to be fast compared to the changes in c_A (similar to the Michaelis-Menten asymptotics), we obtain the quasi-stationary result

$$c_B = \frac{c_0 (c_A/\overline{c})^m}{1 + (c_A/\overline{c})^m} \,, \qquad c_F = \frac{c_0}{1 + (c_A/\overline{c})^m} \,, \tag{21}$$

with the conserved total number of promotor sites $c_0 = c_B + c_F$ and the critical value $\overline{c} = (k_2/k_1)^{1/m}$ for c_A. The function

$$h(c; \overline{c}, m) = \frac{(c/\overline{c})^m}{1 + (c/\overline{c})^m} \,,$$

sometimes called the *Hill function*, makes a transition from small values to values close to 1 around the critical value $c = \overline{c}$. The transition becomes sharper with bigger exponent m (see Fig. 6). Obviously, (21) can be written as

$$c_B = c_0 h(c_A) \,, \qquad c_F = c_0 (1 - h(c_A)) \,. \tag{22}$$

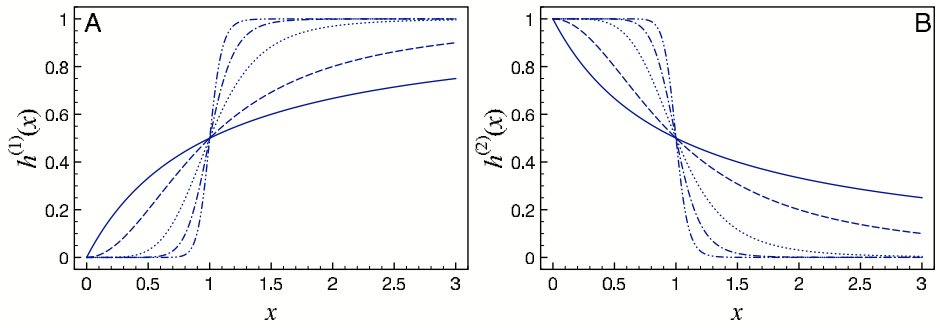

Figure 6: The graph of the Hill function for $m = 1, 2, 5, 10, 20$. Left: $h^{(1)}(x) := h(x; 1, m)$. Right: $h^{(2)}(x) := 1 - h^{(1)}(x)$. Source: [16]

Big values of m are often used because of the experimental observation of a rather sharp switching in gene regulation. However, the above standard derivation of the Hill function is rather questionable, since in general higher order reactions are very unlikely. A possible alternative is *sequential cooperative binding* of A type molecules, where the molecules bind one-by-one and binding of the first drastically facilitates binding of the following ones. This leads to an alternative justification for using the Hill function [16].

The next step is to model transciption, i.e. the production of mRNA with concentration $c_M(t)$. We assume that both free and bound promotor sites contribute and that there is also spontaneous degradation:

$$\frac{dc_M}{dt} = \alpha_F c_F + \alpha_B c_B - \gamma_M c_M \,,$$

with positive parameters α_F, α_B, and γ_M. With (22), the sum of the first two terms on the right hand side,

$$\alpha_F c_F + \alpha_B c_B = c_0 \alpha_F + c_0(\alpha_B - \alpha_F) h(c_a) \,,$$

is an increasing function of c_A for $\alpha_F < \alpha_B$, and a decreasing function of c_A for $\alpha_F > \alpha_B$. In the first case A is an activator, and in the second case a repressor. Typically, α_F and α_B are of strongly different magnitudes, to produce a pronounced effect.

Finally, we use a simple model for translation, i.e. for the protein concentration $c_P(t)$:

$$\frac{dc_P}{dt} = \alpha_M c_M - \gamma_P c_P \,,$$

where we assume that the process is not limited by the availability of ribosomes or the necessary protein ingredients, and that there is also spontaneous degradation of protein.

4.2 Negative feedback – homeostasis

As a simple example, we consider a protein, which acts as a repressor for its own production. This leads to the model

$$\begin{aligned} \frac{dc_M}{dt} &= f(c_P) - \gamma_M c_M \,, \\ \frac{dc_P}{dt} &= \alpha_M c_M - \gamma_P c_P \,, \end{aligned} \tag{23}$$

with the strictly decreasing function

$$f(c_P) := \alpha_F c_0 - (\alpha_F - \alpha_B) c_0 h(c_P) \,, \qquad \alpha_F > \alpha_B \,.$$

It is easily seen that there is a unique steady state $(c_{M,\infty}, c_{P,\infty}) \in \mathbb{R}^2_+$, since the nullclines

$$c_M = \frac{f(c_P)}{\gamma_M} \,, \quad c_M = \frac{\gamma_P c_P}{\alpha_M} \,,$$

are the graphs of a strictly increasing and a strictly decreasing function with a unique intersection (see Fig. 7). Linearization shows that this steady state is locally asymptotically stable.

It is also easily seen that every rectangle of the form

$$[0, c_{M,max}] \times \left[0, \frac{\alpha_M c_{M,max}}{\gamma_P}\right]$$

with $c_{M,max} \geq f(0)/\gamma_M$ is an invariant region for (23) (see Fig. 7). Therefore every trajectory starting with nonnegative initial values is bounded.

The function

$$L(c_M, c_P) = \frac{\alpha_M}{2} \left(c_M - c_{M,\infty}\right)^2 + \int_{c_{P,\infty}}^{c_P} \left(f(c_{P,\infty}) - f(c)\right) dc \,.$$

is a Lyapunov function, since

$$\begin{aligned} \frac{d}{dt} L(c_M, c_P) &= \alpha_M \left(c_M - c_{M,\infty}\right) \frac{dc_M}{dt} + \left(f(c_{P,\infty}) - f(c_P)\right) \frac{dc_P}{dt} \\ &= \alpha_M \left(c_M - c_{M,\infty}\right) \left(f(c_P) - f(c_{P,\infty}) - \gamma_M (c_M - c_{M,\infty})\right) \\ &\quad + \left(f(c_{P,\infty}) - f(c_P)\right) \left(\alpha_M (c_M - c_{M,\infty}) - \gamma_P (c_P - c_{P,\infty})\right) \\ &= -\alpha_M \gamma_M (c_M - c_{M,\infty})^2 - \gamma_P (c_P - c_{P,\infty}) (f(c_{P,\infty}) - f(c_P)) \leq 0 \,, \end{aligned}$$

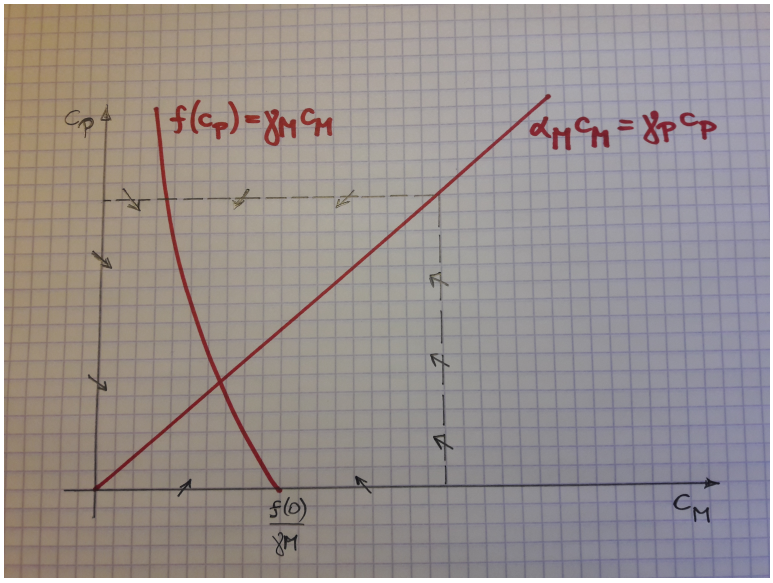

Figure 7: Invariant region for (23).

where we have used that f is decreasing.

The Lyapunov function is strictly convex, nonnegative, and takes its unique minimum at $(c_{M,\infty}, c_{P,\infty})$. Similarly dL/dt only vanishes for $(c_M, c_P) = (c_{M,\infty}, c_{P,\infty})$. Even better, by the boundedness of the trajectories, for every such bounded solution there exists a constant $\kappa > 0$, such that $|f(c_P) - f(c_{P,\infty})| \geq \kappa |c_P - c_{P,\infty}|$, implying

$$L(c_M(t), c_P(t)) \geq \frac{\alpha_M}{2} \left(c_M(t) - c_{M,\infty}\right)^2 + \frac{\kappa}{2} \left(c_P(t) - c_{P,\infty}\right)^2 .$$

So L controls the distance to the equilibrium. On the other hand, by the monotonicity of f,

$$\int_{c_{P,\infty}}^{c_P} \left(f(c_{P,\infty}) - f(c)\right) dc \leq \left(c_P - c_{P,\infty}\right) \left(f(c_{P,\infty}) - f(c_P)\right) ,$$

implying

$$\begin{aligned} \frac{dL}{dt} &\leq -\alpha_M \gamma_M (c_M - c_{M,\infty})^2 - \gamma_P \int_{c_{P,\infty}}^{c_P} \left(f(c_{P,\infty}) - f(c)\right) dc \\ &\leq -\gamma L , \qquad \text{with } \gamma = \min\left\{2\gamma_M, \gamma_P\right\} . \end{aligned}$$

As a consequence of the Gronwall lemma, we have

$$L(t) \leq L(0) e^{-\gamma t}$$

for $t \geq 0$, i.e. exponential convergence of all solutions to the steady state.

This self-regulation by negative feedback, such that the protein concentration is kept at the constant level $c_{P,\infty}$ in a stable way, is an example for *homeostasis.* The fact that this protein level is in a sense optimal, is expected to be a consequence of evolution.

Spatial effects: In the analysis above the fact has been ignored that transcription and translation occur in different places within the cell, i.e. in the nucleus and, respectively, in the ribosomes attached to the endoplasmatic reticulum (see Fig. 1), and that their products have to be transported from one to the other.

We shall try to shed some light on this issue by considering a strongly simplified situation, where we consider the locations of transcription and translation as points connected by a one-dimensional path of length L. Therefore we introduce a one-dimensional position variable $x \in [0, L]$, where $x = 0$ represents the point on the DNA, where transcription takes place, and $x = L$ represents the location of translation. For the transport of mRNA and protein between these two points we assume unbiased diffusion. Obviously, these assumptions are a simplification since the transport actually happens in three-dimensional space and it might by biased by directed transport mechanisms.

We further assume that the production of mRNA happens at $x = 0$ and the production of protein at $x = L$. On the other hand, degradation is assumed to happen everywhere in the interval. For the concentrations $c_M(x, t)$ and $c_P(x, t)$ of mRNA and, respectively, protein this leads to the reaction-diffusion equations (see Section 3)

$$\partial_t c_M = D_M \partial_x^2 c_M - \gamma_M c_M \,, \tag{24}$$

$$\partial_t c_P = D_P \partial_x^2 c_P - \gamma_P c_P \,, \tag{25}$$

for $x \in (0, L)$ with the diffusivities $D_M, D_P > 0$. These are second-order parabolic PDEs, which need boundary conditions. We assume the DNA boundary $x = 0$ to be isolated for the protein and the ribosome boundary $x = L$ to be insulated for the mRNA, which means that the respective diffusive fluxes vanish there:

$$\partial_x c_P(0, t) = \partial_x c_M(L, t) = 0 \,. \tag{26}$$

On the other hand, the production by transcription/translation produces an influx of the respective species:

$$-D_M \partial_x c_M(0, t) = f(c_P(0, t)) \,, \qquad -D_P \partial_x c_P(L, t) = -\alpha_M c_M(L, t) \,, \tag{27}$$

where the meaning of the constant $\alpha_M > 0$ and of the positive-valued decreasing function f are as above. Note the signs in (27), recalling that the left hand sides are (by Fick's law (16)) the fluxes in the positive x-direction.

As in the preceding paragraph, we look for a steady state $(c_{M,\infty}(x), c_{P,\infty}(x))$. The stationary versions of (24) and (25) can be written in the form

$$0 = \partial_x^2 c - \omega^2 c\,. \tag{28}$$

Solving this linear, constant-coefficient ODE is a standard procedure. The ansatz $c(x) = e^{\lambda x}$ leads to the characteristic equation $0 = \lambda^2 - \omega^2$ with the solutions $\lambda = \pm\omega$. As a consequence, any solution of (28) can be written as a linear combination of $e^{\omega x}$ and $e^{-\omega x}$ or, equivalently, of $\sinh(\omega x)$ and $\cosh(\omega x)$ or, third possibility, of $\sinh(\omega(x-L))$ and $\cosh(\omega(x-L))$. Using the non-flux boundary conditions (26), this implies

$$c_{M,\infty}(x) = a_M \cosh\left((x-L)\sqrt{\frac{\gamma_M}{D_M}}\right), \qquad c_{P,\infty}(x) = a_P \cosh\left(x\sqrt{\frac{\gamma_P}{D_P}}\right),$$

with nonnegative constants a_M and a_P to be determined by using the production boundary conditions (27):

$$\begin{aligned} a_M\sqrt{\gamma_M D_M}\sinh\left(L\sqrt{\frac{\gamma_M}{D_M}}\right) &= f(a_P)\,, \\ a_P\sqrt{\gamma_P D_P}\sinh\left(L\sqrt{\frac{\gamma_P}{D_P}}\right) &= \alpha_M a_M\,. \end{aligned}$$

A unique solution $(a_M, a_P) \in (0,\infty)^2$ exists by the same argument as in the preceding paragraph. Thus, there is again a unique steady state. For homeostasis, its dynamic stability is of course important. However, this is definitely much harder to prove than for the spatially homogeneous problem treated before, and we do not attempt to do it here.

4.3 Mutual inhibition – bistability

We consider two proteins, inhibiting each other. As a simplification we assume that the transciption dynamics for both proteins is much faster than the translation dynamics, and that the mRNA densitites therefore can be approximated by quasi-stationary states. The result is a system for the protein densities. Furthermore we make an often used simplifying assumption, which corresponds to letting the Hill exponents pass to infinity:

$$\begin{aligned} \frac{dc_1}{dt} &= f_2(c_2) - \gamma_1 c_1\,, \\ \frac{dc_2}{dt} &= f_1(c_1) - \gamma_2 c_2\,, \end{aligned} \tag{29}$$

with

$$f_j(c_j) = \begin{cases} a_j & \text{for } c_j < \bar{c}_j\,, \\ b_j & \text{else,} \end{cases} \qquad a_j > b_j > 0\,, \qquad j = 1, 2. \tag{30}$$

Note that the discontinuity of f_j takes us out of the standard theory for ordinary differential equations, which requires Lipschitz continuity of the right hand side for existence and uniqueness of solutions. We shall make a theoretical detour to discuss this problem.

Filippov solutions of ODEs with discontinuous right hand side: As a first example, consider the ODE

$$\frac{du}{dt} = \operatorname{sign}(u)\,. \tag{31}$$

An obvious first question is for the value of the derivative, when $u = 0$. The answer of Filippov [5] is to replace the differential equation by a *differential inclusion*. He redefines the sign function as set valued,

$$\widehat{\operatorname{sign}}(u) := \begin{cases} \{-1\} & \text{for } u < 0\,, \\ [-1, 1] & \text{for } u = 0\,, \\ \{1\} & \text{for } u > 0\,, \end{cases} \tag{32}$$

and replaces (31) by

$$\frac{du}{dt} \in \widehat{\operatorname{sign}}(u)\,, \qquad \text{for almost all } t\,. \tag{33}$$

The problem is that the uniqueness of solutions for initial value problems might get lost: The functions

$$u(t) = (t - t_0)_+ \qquad \text{and} \qquad u(t) = -(t - t_0)_+$$

are Filippov solutions of (33) with the initial condition $u(0) = 0$ for every value of $t_0 \geq 0$. This difficulty does not always occur: The problem with the opposite sign,

$$-\frac{du}{dt} \in \widehat{\operatorname{sign}}(u)\,, \qquad u(0) = u_0\,,$$

has the unique Filippov solution

$$u(t) = \begin{cases} u_0 - t \operatorname{sign}(u_0) & \text{for } t < |u_0|\,, \\ 0 & \text{for } t \geq |u_0|\,. \end{cases}$$

The uniqueness can be obtained as a consequence of $\widehat{\operatorname{sign}}(u)$ being the *subdifferential* $\partial|u|$ of a convex function [3], i.e. its monotonicity. This requirement can be generalized to systems

$$\frac{du}{dt} \in \widehat{F}(u)\,,$$

where, for each u, $\widehat{F}(u) \subset \mathbb{R}^d$ is a convex set. However, requiring monotonicity is too restrivtive, since it is not necessary in regions, where $\widehat{F}$ can be represented by a smooth function. Filippov uses *one-sided Lipschitz continuity:* He shows uniqueness of Filippov solutions, if there exists a (one-sided Lipschitz) constant $L \geq 0$, such that

$$(u_1 - u_2) \cdot (F_1 - F_2) \leq L|u_1 - u_2|^2 \,, \qquad \text{for all } u_1, u_2 \text{ and } F_1 \in \widehat{F}(u_1) \,,\ F_2 \in \widehat{F}(u_2) \,.$$

For scalar equations this does not allow upward jumps of the right hand side. Actually, this is still too restrivtive for our purposes. It is easily seen that initial value problems for the differential inclusion

$$\frac{du}{dt} \in 2 + \widehat{\operatorname{sign}}(u) \,,$$

have unique strictly increasing Filippov solutions. Their derivatives just jump from 1 to 3, when they pass through $u = 0$. Obviously, the right hand side is not one-sided Lipschitz. We shall propose a uniqueness criterion adjusted to the situation of the system (29), (30), where the right hand side has jump discontinuities across hypersurfaces.

Let the domain $B \in \mathbb{R}^d$ be the phase space, let $S \subset B$ be a smooth hypersurface with unit normal vector $n(u)$, and let $F : B \setminus S \to \mathbb{R}^d$ be a smooth vector field such that the limits

$$F^{\pm}(u) := \lim_{\varepsilon \searrow 0} F(u \pm \varepsilon n(u))$$

exist for every $u \in S$. Let

$$\widehat{F}(u) := \begin{cases} \{F(u)\} \,, & \text{for } u \in B \setminus S \,, \\ \{\alpha F^+(u) + (1-\alpha) F^-(u) : \, 0 \leq \alpha \leq 1\} \,, & \text{for } u \in S \,. \end{cases}$$

This means that F has jump discontinuities along S, and we complete the graph by connecting the endpoints of the jumps by straight lines, just as in (32). We propose the following *conjecture:* If $\widehat{F}$ as defined above satisfies for every $u \in S$ the property

$$0 \in n(u) \cdot \widehat{F}(u) \quad \Longrightarrow \quad n(u) \cdot F^-(u) \geq 0 \text{ and } n(u) \cdot F^+(u) \leq 0 \,, \tag{34}$$

then initial value problems for

$$\frac{du}{dt} \in \widehat{F}(u)$$

with $u(0) \in B$ have unique Filippov solutions. The interpretation of (34) is the following: *If a Filippov solution has the option to stay on S, then this has to be the only option.*

For applying these ideas to (29), we note that the above assumptions are violated at the point $(\overline{c}_1, \overline{c}_2)$, where the discontinuities cross. We therefore

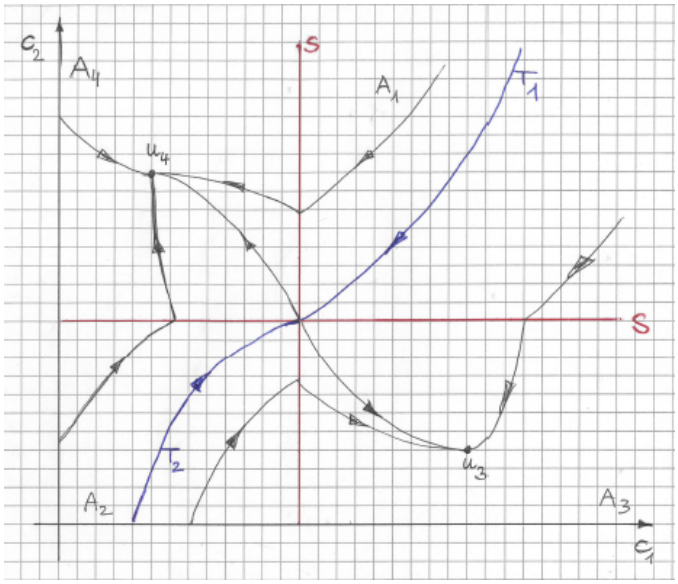

Figure 8: Phase portrait of the system (29).

take this point out of the phase space for the moment:

$$\begin{aligned} B &:= [0,\infty)^2 \setminus \{(\overline{c}_1, \overline{c}_2)\}\,, \\ S &:= \{(c_1,c_2) \in B : \, c_1 = \overline{c}_1 \text{ or } c_2 = \overline{c}_2\}\,. \end{aligned}$$

We therefore obtain

$$\widehat{F}(c_1,c_2) = \begin{cases} \{(f_2(c_2) - \gamma_1 c_1, f_1(c_1) - \gamma_2 c_2)\}\,, & \text{for } (c_1,c_2) \in B \setminus S\,, \\ \{f_2(c_2) - \gamma_1 c_1\} \times [b_1 - \gamma_2 c_2, a_1 - \gamma_2 c_2]\,, & \text{for } c_1 = \overline{c}_1\,, \\ [b_2 - \gamma_1 c_1, a_2 - \gamma_1 c_1] \times \{f_1(c_1) - \gamma_2 c_2\}\,, & \text{for } c_2 = \overline{c}_2\,. \end{cases}$$

We consider the situation

$$b_2 < \gamma_1 \overline{c}_1 < a_2\,, \qquad b_1 < \gamma_2 \overline{c}_2 < a_1\,, \tag{35}$$

and note that $B \setminus S$ is the union of four connected components $A_1, \ldots, A_4$ (see Fig. 8), in each of which the equations are very simple and can be solved explicitly.

For example, in $A_1 := \{c_1 > \overline{c}_1,\, c_2 > \overline{c}_2\}$ we have

$$\frac{dc_1}{dt} = b_2 - \gamma_1 c_1\,, \qquad \frac{dc_2}{dt} = b_1 - \gamma_2 c_2\,,$$

with both right hand sides being negative by (35). As a consequence, every solution starting in A_1 leaves it in finite time. More precisely, there is a special trajectory

$$T_1 := \left\{ \left(\frac{b_2}{\gamma_1} + \left(\overline{c}_1 - \frac{b_2}{\gamma_1} \right) e^{-\gamma_1 t}, \frac{b_1}{\gamma_2} + \left(\overline{c}_2 - \frac{b_1}{\gamma_2} \right) e^{-\gamma_2 t} \right), t < 0 \right\} ,$$

reaching the forbidden point $(\overline{c}_1, \overline{c}_2)$ in finite time. Every trajectory starting below T_1 leaves A_1 towards $A_3 := \{c_1 > \overline{c}_1,\, c_2 < \overline{c}_2\}$, and every trajectory starting above T_1 leaves A_1 towards $A_4 := \{c_1 < \overline{c}_1,\, c_2 > \overline{c}_2\}$. The dynamics in $A_2 := \{c_1 < \overline{c}_1,\, c_2 < \overline{c}_2\}$ is analogous to that in A_1, more or less only with the signs reversed. There is again a special trajectory, now called T_2, splitting the trajectories in A_2 into two parts moving towards A_3 or A_4.

It is easily seen that (34) holds on the four parts of S, since the left hand side of the implication is never true. This means that when the trajectories leave A_1 or A_2 they can be continued in a unique way in A_3 or A_4.

In A_3 we have

$$\frac{dc_1}{dt} = a_2 - \gamma_1 c_1 \,, \qquad \frac{dc_2}{dt} = b_1 - \gamma_2 c_2 \,,$$

with the stable steady state $u_3 = (a_2/\gamma_1, b_1/\gamma_2)$. All trajecories starting in A_3 or entering A_3 through S converge to u_3. Analogously, there is a stable steady state $u_4 = (b_2/\gamma_1, a_1/\gamma_2) \in A_4$.

As a conclusion, we have the result that all trajectories starting below the union of T_1 and T_2 converge to u_3, and all trajectories starting above converge to u_4.

The trajectories T_1 and T_2 in A_2 reach the forbidden point $(\overline{c}_1, \overline{c}_2)$ in finite time. An appropriate definition of the right hand side at the forbidden point would be

$$\widehat{F}(\overline{c}_1, \overline{c}_2) = [a_2 - \gamma_1 c_1, b_2 - \gamma_1 c_1] \times [a_1 - \gamma_2 c_2, b_1 - \gamma_2 c_2] \,,$$

containing the origin, which means that a Filippov solution may stay there. However, there is one trajectory in A_3 and one in A_4, leaving this point with finite speed, meaning that all solutions starting on T_1 and T_2 are not determined uniquely. The union of T_1 and T_2 separates the phase space into two parts, the domains of attraction of the two stable steady states u_3 and u_4. The consequence of this bistability is that the cell can be switched from one state to the other by a short perturbation moving the state away from one steady state into the domain of attraction of the other.

4.4 Activation, inhibition, and delays – periodic cycles

We again consider two proteins, however, now we assume that protein 1 activates protein 2, but protein 2 inhibits protein 1. While we again make the simplification for fast transcription (compared to translation), we assume that there is a time delay between the moment, where an activator or a repressor binds to the gene, and the completion of the transcription and translation processes. This leads to a model of the form [14]

$$\begin{aligned} \frac{dc_1}{dt}(t) &= f_2(c_2(t-\tau_1)) - \gamma_1 c_1(t)\,, \\ \frac{dc_2}{dt}(t) &= f_1(c_1(t-\tau_2)) - \gamma_2 c_2(t)\,, \end{aligned} \tag{36}$$

with a decreasing function $f_2 > 0$, an increasing function $f_1 > 0$, and the delays $\tau_1, \tau_2 > 0$. This system of *delay-differential equations* has mathematical properties strongly different from ordinary differential equations. For example, the required initial data are not just $c_1(0)$ and $c_2(0)$, but the values of $c_1(t)$ for $-\tau_2 \le t \le 0$ and the values of $c_2(t)$ for $-\tau_1 \le t \le 0$ need to be prescribed. By setting $u(t) = c_1(t)$, $v(t) = c_2(t-\tau_1)$, we reduce to a system with only one delay:

$$\begin{aligned} \frac{du}{dt} &= f_2(v) - \gamma_1 u\,, \\ \frac{dv}{dt} &= f_1(u(t-\tau)) - \gamma_2 v\,, \end{aligned} \tag{37}$$

with $\tau = \tau_1 + \tau_2$, and the argument t has been skipped. In spite of the above mentioned difficulties, we try to analyze the long time behavior with ideas from ordinary differential equations. By the properties of f_1 and f_2 there is a unique steady state $(\overline{u}, \overline{v}) \in (0,\infty)^2$, satisfying $f_2(\overline{v}) = \gamma_1 \overline{u}$, $f_1(\overline{u}) = \gamma_2 \overline{v}$.

As usual in dynamical systems we try to understand the stability of the steady state by linearization. This means that we make the replacements $u \to \overline{u} + u$ and $v \to \overline{v} + v$, where the new u and v are considered as small perturbations, and then we replace the nonlinear terms by their linear Taylor polynomial. For the right hand side of the second equation this gives

$$f_1(u(t-\tau)) - \gamma_2 v \to f_1(\overline{u} + u(t-\tau)) - \gamma_2(\overline{v} + v) \approx f_1'(\overline{u}) u(t-\tau) - \gamma v\,.$$

With the corresponding computation for the first equation, the linearization of (37) at the steady state is given by

$$\begin{aligned} \frac{du}{dt} &= f_2'(\overline{v}) v - \gamma_1 u\,, \\ \frac{dv}{dt} &= f_1'(\overline{u}) u(t-\tau) - \gamma_2 v\,. \end{aligned} \tag{38}$$

The next step is also motivated from the theory of ordinary differential equations, but it is not obvious to be appropriate here: We make the ansatz

$$u(t) = e^{\lambda t} u_0 \,, \qquad v(t) = e^{\lambda t} v_0 \,,$$

which would produce an eigenvalue problem for a system of ordinary differential equations. Here it leads to

$$\begin{pmatrix} \gamma_1 + \lambda & -f_2'(\overline{v}) \\ -f_1'(\overline{u}) e^{-\lambda\tau} & \gamma_2 + \lambda \end{pmatrix} \begin{pmatrix} u_0 \\ v_0 \end{pmatrix} = 0$$

Although this is not an eigenvalue problem, the same kind of argument can be used: This linear homogeneous system for (u_0, v_0) has nontrivial solutions, only if the coefficient matrix is nonregular, i.e. its determinant vanishes:

$$(\gamma_1 + \lambda)(\gamma_2 + \lambda) + D e^{-\lambda\tau} = 0 \,, \qquad \text{with } D = -f_1'(\overline{u}) f_2'(\overline{v}) \geq 0 \,. \tag{39}$$

Now the idea is to vary the delay τ. Starting with the ODE situation $\tau = 0$, we easily observe that in this case the eigenvalues

$$\lambda = -\frac{\gamma_1 + \gamma_2}{2} \pm \sqrt{\frac{(\gamma_1 + \gamma_2)^2}{4} - \gamma_1\gamma_2 - D}$$

all have negative real parts because of $D \geq 0$. In the situation without delay, the steady state is stable (at least from the linearized point of view). Since we expect the solutions λ of (39) to depend continuously on τ, linearized instability is only possible, if for some value $\tau = \tau_0 > 0$ a purely imaginary eigenvalue $\lambda = i\omega_0$ occurs. Substitution into (39),

$$-\omega_0^2 + i\omega_0(\gamma_1 + \gamma_2) + \gamma_1\gamma_2 + D(\cos(\omega_0\tau_0) - i\sin(\omega_0\tau_0)) = 0 \,,$$

and separation of real and imaginary parts gives

$$\begin{aligned} &\omega_0^2 - \gamma_1\gamma_2 - D\cos(\omega_0\tau_0) = 0 \,, \\ &\omega_0(\gamma_1 + \gamma_2) - D\sin(\omega_0\tau_0) = 0 \,. \end{aligned} \tag{40}$$

Elimination of τ_0,

$$\omega_0^4 + \omega_0^2(\gamma_1^2 + \gamma_2^2) + \gamma_1^2\gamma_2^2 = D^2 \,,$$

shows that this can only occur under the assumption

$$D = |f_1'(\overline{u}) f_2'(\overline{v})| > \gamma_1\gamma_2 \,, \tag{41}$$

whence

$$\omega_0^2 = -\frac{\gamma_1^2+\gamma_2^2}{2} + \sqrt{\left(\frac{\gamma_1^2+\gamma_2^2}{2}\right)^2 + D^2 - \gamma_1^2\gamma_2^2} > 0\,.$$

We conclude (without a reliable theoretical basis, however) that, when (41) fails, the steady state is stable for all $\tau > 0$. When on the other hand (41) holds, there exists a smallest positive value

$$\tau_0 = \frac{1}{\omega_0}\arctan\left(\frac{\omega_0(\gamma_1+\gamma_2)}{\omega_0^2-\gamma_1\gamma_2}\right)\,,$$

such that (40) holds, and there exists a pair of complex conjugate imaginary values for $\lambda(\tau_0)$. Then implicit differentiation of (39) with respect to τ shows (after some computation) that

$$\mathrm{Re}\left(\lambda'(\tau_0)\right) > 0\,,$$

implying that the steady state looses its stability at $\tau = \tau_0$. The fact that a pair of complex conjugate eigenvalues crosses the imaginary axis indicates the occurrence of a *Hopf bifurcation*, creating a stable limit cycle, i.e. a solution periodic in time, for $\tau > \tau_0$.

An example for periodic fluctuations induced by gene regulation are *circadian rythms* [17], responsible, for example, for jet lag.

Theoretical excursion on the Hopf bifurcation in ODEs: We consider the example

$$\dot r = r(\mu - r^2)\,, \qquad \dot\varphi = 1\,, \tag{42}$$

of a dynamical system in $\mathbb{R}^2$, written in terms of polar coordinates (r,φ), containing a parameter $\mu \in \mathbb{R}$. In the equation for r, $\mu = 0$ is a *bifurcation point*, since the steady state $r = 0$ is stable for $\mu < 0$ and unstable for $\mu > 0$. For $\mu > 0$ there are two additional steady states $r = \pm\sqrt{\mu}$, both stable (see Fig. 9). Of course in the polar coordinate interpretation, only the positive one is relevant. This situation is called a *pitchfork bifurcation*.

What does this mean for the dynamical system in $\mathbb{R}^2$? Obviously the origin is a stable equilibrium for $\mu < 0$. For $\mu > 0$ the radius r converges to a positive value, whereas in the angular direction there is a constant angular velocity. The dynamics approaches a periodic solution, called a *limit cycle* (see Fig. 10).

In terms of Euclidean coordinates $(x,y) = r(\cos\varphi, \sin\varphi)$, the system (42) becomes

$$\dot x = x(\mu - x^2 - y^2) - y\,, \qquad \dot y = y(\mu - x^2 - y^2) + x\,.$$

The coefficient matrix for the linearization at the origin,

$$\begin{pmatrix} \mu & -1 \\ 1 & \mu \end{pmatrix}\,,$$

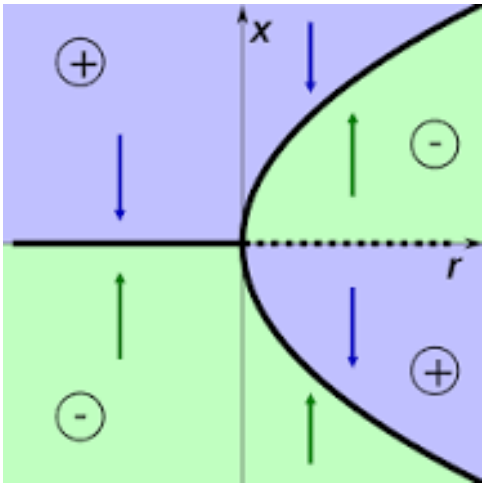

Figure 9: Bifurcation diagram for the pitchfork bifurcation in the r-equation in (42). Notation: x should be r, and r should be μ. Source: `wikipedia`.

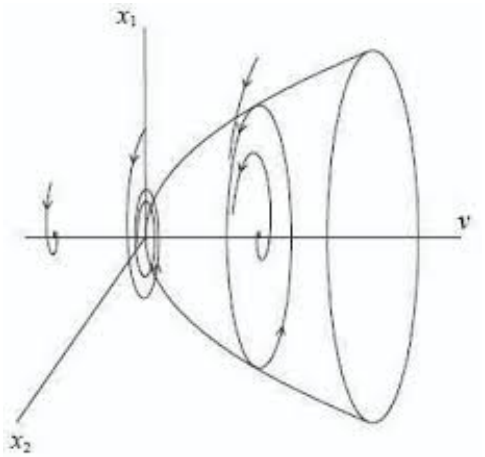

Figure 10: Bifurcation diagram for the Hopf bifurcation. Notation: ν should be μ. Source: C.C. Karaaslani, Bifurcation Analysis and its Applications, DOI: 10.5772/50075

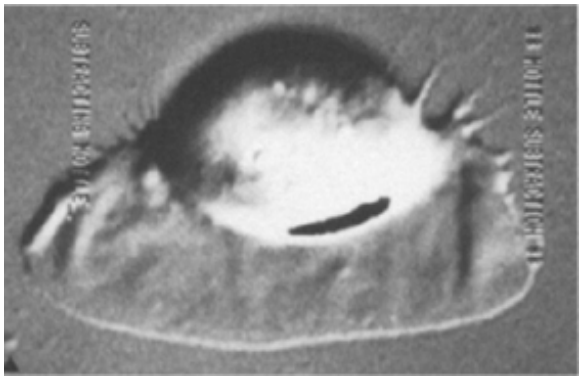

Figure 11: A fish keratocyte crawling on a flat substrate (downwards in the picture). The flat part in front is the lamellipodium. All other important cell organelles are in the thick part behind.

has the eigenvalues $\mu \pm i$. When μ changes sign, a pair of complex conjugate eigenvalues crosses the imaginary axis. This is called a *Hopf bifurcation*. While a steady state loses its stability a stable limit cycle appears.

5 Cell crawling by cytoskeleton dynamics

5.1 The lamellipodium

When brought into contact with a flat substrate, many cell types build a thin (almost two-dimensional) protrusion, called *lamellipodium*, which adheres to the substrate (see Fig. 11). This structure is supported by a network of polymer filaments consisting of molecules of *actin,* one of the most important proteins, occurring in every cell type. Actin filaments are part of the *cytoskeleton,* built from three types of protein filaments: actin filaments, *microtubuli,* and *intermediate filaments.* The cytoskeleton shares some of its function with the skeleton of animals, such as mechanical support and movement. However, there are important differences, since the cytoskeleton is a very dynamic structure, also important for morphological changes of the cell and as an intracellular transportation network.

Although in many cases the lamellipodium has a stable shape for longer periods, its actin network is very dynamic with permanent filament polymerization and depolymerization. The filaments are polar (i.e. oriented) with their so called *barbed ends* towards the outer leading edge of the lamellipodium, where they are permanently elongated by polymerization. At

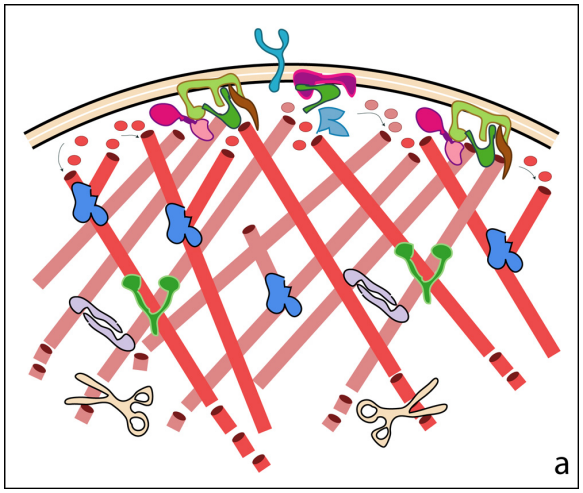

Figure 12: Cartoon of the actin filament meshwork in the lamellipodium.

the inner *pointed ends,* on the other hand, depolymerization mechanisms dominate. The actin monomers diffuse through the cytoplasm outward to the leading edge. The mechanical stability of the structure comes from the fact that it is branched and from cross-linking proteins, connecting crossing filaments.

Adhesion to the substrate is the result of binding and unbinding of cytoskeleton attached transmembrane proteins to the substrate. This process will be investigated first.

5.2 Friction from building and breaking elastic connections

We shall call a rigid piece of the lamellipodium a *sailing ship.* Chemical connections between the cytoskeleton and the substrate will be called *anchors.* We assume that the wind blows in the x-direction, exerting a time dependent force $F(t)$ on the ship. The ship (also called *Monk's sail boat*) is equipped with a large number N of anchors on elastic ropes, which break loose at random times and are re-attached, again at random times. How does the ship move under the assumption that there is always a quasistationary balance between the force $F(t)$ and the sum of the elastic forces by the ropes of the attached anchors?

For the computation of the elastic force of an anchor, we denote the position of the ship at time t by $x(t) \in \mathbb{R}$ and introduce the *age* a of an anchor, i.e. the time which has passed since the anchor has been attached.

Figure 13: Adrian Monk.

The anchor rope then has the length $x(t)-x(t-a)$ at time t. Using a linear elasticity law, the elastic force is given by $k(x(t)-x(t-a))$ with a positive elasticity constant k. The randomness of attaching and de-attaching an anchor will be described by the age dependent distribution $\varrho(a,t)$, meaning that the integral

$$\int_{\underline{a}}^{\overline{a}} \varrho(a,t)da$$

gives the probability that at time t the anchor is attached with an age between $\underline{a}$ and $\overline{a}$. Multiplication of this value by N gives the expected number at time t of anchors with an age between $\underline{a}$ and $\overline{a}$. The balance between the expected total friction force and the force induced by the wind leads to the equation

$$F(t) = Nk \int_0^\infty (x(t)-x(t-a))\varrho(a,t)da\,. \tag{43}$$

This can be seen as an integral equation for the determination of $x(t)$. It remains to compute $\varrho(a,t)$. Attachment, de-attachment, and aging of attached anchors is descibed by an age-structured population model:

$$\partial_t\varrho + \partial_a\varrho = -\zeta\varrho\,, \quad \varrho(0,t) = \beta\left(1-\int_0^\infty \varrho(a,t)da\right)\,. \tag{44}$$

The left hand side of the differential equation describes aging, the right hand side de-attachment with rate constant ζ, and the boundary condition describes attachment with a rate proportional to the probability of the anchor to be free.

For a nondimensionalisation, we note that $1/\zeta$ is the mean lifetime of anchors. Reference values F_0 for the force and t_0 for time are chosen such that, when $F(t)$ is rescaled with these values, the resulting function takes

moderate values and varies moderately. The main scaling assumptions are that the mean lifetime of anchors is small compared to t_0, and that the attachment rate is of the same order of magnitude as the de-attachment rate. This motivates the definition of the small dimensionless parameter $\varepsilon = 1/(t_0\zeta)$. Finally, we choose a characteristic length

$$x_0 = \frac{F_0 t_0 \zeta}{Nk}\,.$$

Now the rescaling

$$a \to \frac{a}{\zeta}\,, \quad t \to t_0 t\,, \quad x \to x_0 x\,, \quad \varrho \to \zeta\varrho\,, \quad F \to F_0 F\,, \quad \beta \to \zeta\beta\,,$$

transforms (43), (44) into

$$F(t) = \int_0^\infty \frac{x(t) - x(t-\varepsilon a)}{\varepsilon}\varrho(a,t)da\,, \tag{45}$$

$$\varepsilon\partial_t\varrho + \partial_a\varrho = -\varrho\,, \quad \varrho(0,t) = \beta\left(1 - \int_0^\infty \varrho(a,t)da\right)\,. \tag{46}$$

After the formal limit $\varepsilon \to 0$, the differential equation in (46) implies

$$\varrho(a,t) = \varrho(0,t)e^{-a}\,.$$

Substitution in the boundary condition gives

$$\varrho = \frac{\beta}{1+\beta}e^{-a}\,.$$

With this, the limit of (45) becomes

$$F(t) = \int_0^\infty \dot{x}(t)a\varrho(a)da = \kappa\dot{x}(t)\,,$$

i.e., the force produced by the anchors becomes a linear friction force with the friction coefficient $\kappa = \beta/(1+\beta)$.

Although the formal asymptotics as $\varepsilon \to 0$ has been very easy, the corresponding rigorous theory is surprisingly difficult, see [12].

Digression: variational formulation – gradient flows vs. friction. Consider again (45). It is an easy observation that for given $x(t-\varepsilon a)$, $a > 0$, the value of $x(t)$ can be determined by a minimization:

$$x(t) = \mathrm{argmin}_{y\in\mathbb{R}}\left(\int_0^\infty \frac{(y - x(t-\varepsilon a))^2}{2\varepsilon}\varrho(a,t)da - yF(t)\right)\,, \tag{47}$$

the term in the paranthesis being a quadratic polynomial in y. In the limit $\varepsilon \to 0$ we have obtained $\kappa \dot{x}(t) = F(t)$, which can also be obtained from the similar limit

$$x(t) = \lim_{h \to 0} \operatorname{argmin}_{y \in \mathbb{R}} \left(\kappa \frac{(y - x(t-h))^2}{2h} - yF(t) \right) .$$

This corresponds to solving the differential equation by the *implicit Euler method*

$$\kappa \frac{x_h(t) - x_h(t-h)}{h} = F(t) ,$$

('implicit' since the right hand side is evaluated at the 'new' time t and not the 'old' time $t - h$).

More generally: Let $(\mathcal{H}, \langle \cdot, \cdot \rangle)$ be a Hilbert space, let $E : \mathcal{H} \to \mathbb{R}$ be a *potential energy functional*, and let ∇E be the 'gradient' (actually the Hilbert space (Riesz) representation of the Fréchet derivative) of E in the sense $E(x+y) = E(x) + \langle \nabla E(x), y \rangle + o(\|y\|)$ as $\|y\| \to 0$. Then the abstract ODE

$$\kappa \dot{x} = -\nabla E(x) , \tag{48}$$

is called the *gradient flow* for E with friction coefficient $\kappa > 0$. The implicit Euler method

$$\kappa \frac{x_h(t) - x_h(t-h)}{h} = -\nabla E(x_h(t)) ,$$

has the variational formulation

$$x_h(t) = \operatorname{argmin}_{y \in \mathcal{H}} \left(\kappa \frac{\|y - x_h(t-h)\|^2}{2h} + E(y) \right) . \tag{49}$$

The gradient flow has mathematical importance as a method to find minima of E, note that (48) implies

$$\frac{dE(x)}{dt} = \langle \nabla E(x), \dot{x} \rangle = -\frac{1}{\kappa} \|\nabla E(x)\|^2 , \tag{50}$$

but it can also serve as a model, where forces are on the one hand derived from a potential energy and, on the other hand, from friction. Note that the first term in the parenthesis can be interpreted as the potential energy of anchors with a fixed life time h. Note also that the formulation (49) with subsequent limit $h \to 0$ can be understood as the definition of the gradient flow or of friction, even if the underlying state space is not a Hilbert space, e.g. a submanifold of a Banach space.

5.3 A one-dimensional model for cell spreading

If a cell builds a ring shaped lamellipodium on a flat substrate, where there is always polymerization in the outward direction and adhesion with the substrate, the area covered by the cell tends to get bigger and bigger. This is counteracted by the tension of the cell membrane. We want to investigate the balance between these effects. For simplicity we assume a one-dimensional model, which can be understood as describing a one-dimensional cross-section.

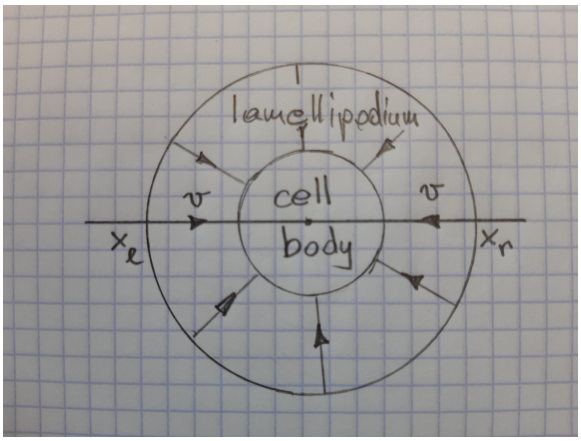

Figure 14: Cell with ring shaped lamellipodium and one-dimensional section.

Along the x-axis let $x_l(t)$ and $x_r(t)$ denote the left and, respectively, the right edge of the cell. Assuming the membrane tension to increase linearly with the cell width exceeding an equilibrium value L, the tension force can be modeled as $\mu(x_r - x_l - L)$ acting on x_l and the opposite acting on x_r. If polymerization of the actin filaments causes an elongation speed v, then the monomers in the lamellipodium on the left hand side move relative to the substrate with velocity $\dot{x}_l + v$, and in the lamellipodium on the right hand side with velocity $\dot{x}_r - v$. If adhesion creates a friction force as described in the previous paragraph, then the force balances for the two lamellipodia can be written as

$$\begin{aligned} -\kappa(\dot{x}_r - v) - \mu(x_r - x_l - L) &= 0\,, \\ -\kappa(\dot{x}_l + v) + \mu(x_r - x_l - L) &= 0\,. \end{aligned}$$

Adding the two equations gives $\dot{x}_r + \dot{x}_l = 0$, meaning that the center $(x_r +$

$x_l)/2$ of the cell does not move. The difference of the equations gives

$$\kappa \frac{d}{dt}(x_r - x_l) = -2\mu(x_r - x_l) + 2\mu L + 2\kappa v \,,$$

a differential equation for the width of the cell, implying

$$\lim_{t\to\infty} (x_r(t) - x_l(t)) = L + \frac{\kappa v}{\mu} \,,$$

a steady state length increased above the equilibrium value by the polymerization dynamics.

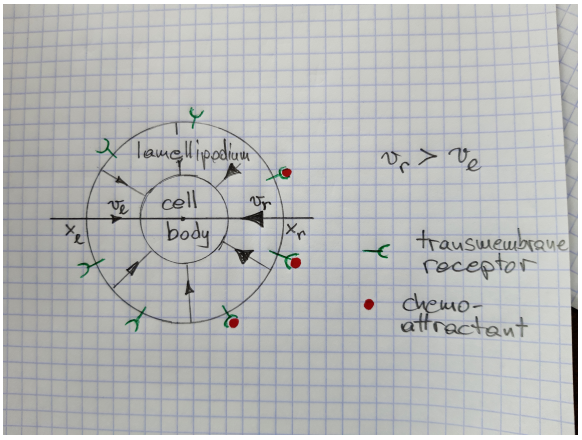

Figure 15: Cell with ring shaped lamellipodium and one-dimensional section. Increased polymerization on the right, stimulated by chemo-attractant binding.

5.4 Chemotaxis

Very generally, *chemotaxis* is the movement of individuals directed by chemical signals. We shall describe a very simple, but not unrealistic model, how this can happen. By membrane receptors and transmembrane signaling, many cell types are able to sense variations in the concentration of extracellular chemicals along their surface. By intracellular chemical pathways this can lead to activation or deactivation of protein activity with a directional bias. For example, in the framework of the model of the preceding paragraph, the cell might sense a chemical concentration, which is higher on the right than on the left. This might lead to different polymerization

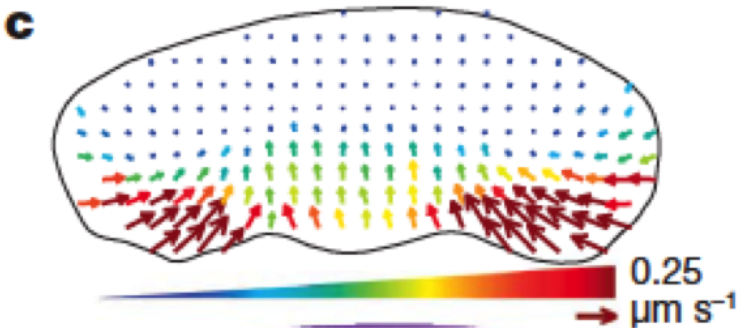

Figure 16: Measurement of the velocity relative to the substrate of the cytoskeleton of a fish keratocyte moving upwards.

speeds v_r and v_l in the right and, respectively, the left lamellipodium, say with $v_r > v_l$. Taking this into account in the preceding model, we get

$$-\kappa(\dot{x}_r - v_r) - \mu(x_r - x_l - L) = 0\,,$$
$$-\kappa(\dot{x}_l + v_l) + \mu(x_r - x_l - L) = 0\,.$$

This produces a cell moving with the speed

$$\frac{\dot{x}_r + \dot{x}_l}{2} = \frac{v_r - v_l}{2}$$

to the right, i.e. in the direction of increasing chemical concentration. For its width we have, not very surprisingly,

$$\lim_{t\to\infty}(x_r(t) - x_l(t)) = L + \frac{\kappa(v_r + v_l)}{2\mu}\,,$$

5.5 Length distribution of actin filaments

An obvious consequence of the model in the previous paragraph is that the speed of the cytoskeleton relative to the substrate is the same in the front part of the lamellipodium on the right and in the rear part on the left, i.e. $|\dot{x}_r - v_r| = |\dot{x}_l + v_l|$. This contradicts experimental results, see Fig. 17. An explanation is that the higher polymerization speed in the front part produces longer filaments and therefore a wider lamellipodium with stronger friction than on the rear side.

This motivates to study the length distribution of actin filaments. We assume that at the leading edge the barbed ends of the filaments are attached and polymerize with a given speed v. Among several possible types

of depolymerization mechanisms, we describe *severing,* which means that filaments can be cut at any position. The cut-off piece is assumed not to play a role any more and is therefore disregarded. Actually it is expected to be completely decomposed very fast. The severing process is modeled as stochastic with randomly chosen severing times and randomly chosen severing positions. This is an example for a *compound Poisson process.*

Compound Poisson processes: A compound Poisson process is a stochastic process, where random jumps in a state space occur at random times, where the jump times are Poisson distributed and the distribution of the jumps is prescribed. We only present the evolution of the probability density, and we start with a finite state space, say $\{1,\dots,n\}$. The probability of the state i at time t is denoted by $p_i(t)$, $i=1,\dots,n$. Thus, $p_i(t)\geq 0$ and $\sum_{i=1}^n p_i(t)=1$ for all t. For the evolution of the probability distribution we postulate the *master equation*

$$\frac{dp_i}{dt}=\sum_{j=1}^n W_{j\to i}\,p_j-\lambda_i p_i\,,\qquad \text{with } \lambda_i=\sum_{j=1}^n W_{i\to j}\,,\quad i=1,\dots,n\,,$$

and with given $W_{i\to j}\geq 0$, $i,j=1,\dots,n$ (assuming $W_{i\to i}=0$). The interpretation is that λ_i is the Poisson parameter for jumping away from state i, and that, in case a jump away from state i occurs, $k_{i\to j}:=W_{i\to j}/\lambda_i$ is the probability to jump from i to j. Note that $(k_{i\to j})_{j=1,\dots,n}$ is a probability distribution on the state space.

The first order chemical reaction networks considered in Section 2 are an example. In the system (6) the unknown $c_i(t)$ could also be interpreted as the probability of an individual molecule, changing between the species by the chemical reactions, to belong to the species i at time t.

More generally, let the state space $(S,d\mu)$ be a general measure space and $p(s,t)$, $s\in S$, $t\in\mathbb{R}$, the probability density for a compound Poisson process. Then the master equation is given by

$$\begin{aligned}\partial_t p(s,t) &= \int_S W(s'\to s)p(s',t)d\mu(s')-\lambda(s)p(s,t)\,,\\ &\qquad \text{with } \lambda(s)=\int_S W(s\to s')d\mu(s')\,.\end{aligned}$$

For actin filament severing, we assume that the Poisson parameter for a filament to get cut is proportional to its length $s\in S=(0,\infty)$ (S equipped with the Lebesgue measure), i.e. $\lambda(s)=\kappa_{sev}s$, $\kappa_{sev}>0$. Cutting a filament means a jump to a smaller length s', where we assume a uniform distribution of the cutting position s' on $[0,s]$, i.e. $k(s\to s')=H(s-s')/s$ with the Heavyside function H. This gives $W(s\to s')=\kappa_{sev}H(s-s')$ and the master

equation

$$\begin{aligned}\partial_t p &= \mathcal{K}(p) := \kappa_{sev} \int_0^\infty \big(H(s'-s)p' - H(s-s')p\big)\, ds' \\ &= \kappa_{sev} \left(\int_s^\infty p' ds' - sp \right) ,\end{aligned}$$

where the abbreviation p' means evaluation at s'. With this model filaments would get shorter and shorter and the probability distribution would concentrate more and more at $s = 0$. This can be deduced from the evolution of the mean length $\overline{s}(t) := \int_0^\infty sp(s,t)ds$:

$$\begin{aligned}\frac{d\overline{s}}{dt} &= \kappa_{sev} \left(\int_0^\infty s \int_s^\infty p' ds'\, ds - \int_0^\infty s^2 p ds \right) \\ &= \kappa_{sev} \left(\int_0^\infty \frac{s^2}{2} p ds - \int_0^\infty s^2 p ds \right) = -\frac{\kappa_{sev}}{2} \int_0^\infty s^2 p ds = -\frac{\kappa_{sev}}{2}\, \overline{s^2}\end{aligned}$$

For the second equality we have integrated by parts and assumed that $s^2 p(s) \to 0$ as $s \to \infty$. The Jensen[2] (or Cauchy-Schwarz) inequality $\overline{s}^2 \le \overline{s^2}$ implies the differential inequality

$$\frac{d\overline{s}}{dt} \le -\frac{\kappa_{sev}}{2}\, \overline{s}^2 .$$

The comparison theorem for ODEs implies that $\overline{s}$ can be estimated by the solution of the corresponding differential equation:

$$\overline{s}(t) \le \frac{\overline{s}(0)}{1 + \kappa_{sev} t/2} , \qquad t \ge 0 .$$

So filaments get shorter and shorter. This effect can be balanced by polymerization, which we assume to happen with fixed given speed v, leading to the complete model

$$\partial_t p + v \partial_s p = \mathcal{K}(p) .$$

Because of $v > 0$, a boundary condition at $s = 0$ is needed. We assume that no new filaments are nucleated, leading to

$$p(0,t) = 0 , \qquad \text{for all } t .$$

At first glance, this partial integro-differential equation looks rather complicated. It helps to rewrite it in conservation form:

$$\partial_t p + \partial_s \left(vp - \kappa_{sev} s \int_s^\infty p' ds' \right) = 0 .$$

[2]Roughly: $\Phi(\overline{x}) \le \overline{\Phi(x)}$ for every convex real valued Φ and any kind of average $x \mapsto \overline{x}$.

We look for an equilibrium distribution $p_\infty(s)$ with vanishing flux:

$$\frac{vp_\infty}{\kappa_{sev}s} = \int_s^\infty p'_\infty ds' \,.$$

Taking the derivative of this equation with respect to s leads to a first order linear ordinary differential equation

$$\frac{dq}{ds} = -\frac{\kappa_{sev}}{v} sq \qquad \text{for } q = \frac{p_\infty}{s} \,,$$

which can be solved explicitly:

$$p_\infty(s) = \frac{\kappa_{sev}s}{v} \exp\left(-\frac{\kappa_{sev}s^2}{2v}\right) \,, \tag{51}$$

where the integration constant has been chosen such that p_∞ is a probability distribution. Analogously to Section 2, we show the stability of the equilibrium by using the Lyapunov function

$$L(t) = \frac{1}{2}\int_0^\infty p_\infty u^2 ds \,, \qquad \text{with } u(s,t) = \frac{p(s,t) - p_\infty(s)}{p_\infty(s)} \,,$$

satisfying

$$\frac{dL}{dt} = \int_0^\infty u(\mathcal{K}(p) - v\partial_s p) ds \,.$$

We compute

$$\begin{aligned}
\int_0^\infty u\partial_s p \, ds &= \int_0^\infty u\partial_s(p_\infty u + p_\infty) ds \\
&= \int_0^\infty (u^2+u)\partial_s p_\infty \, ds + \int_0^\infty p_\infty \partial_s\left(\frac{u^2}{2}\right) ds \\
&= \int_0^\infty \left(\frac{u^2}{2} + u\right)\partial_s p_\infty \, ds \,,
\end{aligned}$$

which gives

$$\begin{aligned}
\frac{dL}{dt} &= \int_0^\infty u\mathcal{K}(p) ds - \int_0^\infty \left(\frac{u^2}{2}+u\right)\mathcal{K}(p_\infty) ds \\
&= \int_0^\infty u\mathcal{K}(p_\infty u) ds - \int_0^\infty \frac{u^2}{2}\mathcal{K}(p_\infty) ds \\
&= \kappa_{sev}\int_0^\infty\int_0^\infty \left[H(s'\to s)p'_\infty\left(u'u - \frac{u^2}{2}\right) - H(s\to s')p_\infty\frac{u^2}{2}\right] ds' ds \,.
\end{aligned}$$

Interchanging s and s' in the second part leads to

$$\frac{dL}{dt} = -\frac{\kappa_{sev}}{2}\int_0^\infty\int_0^\infty H(s'\to s)p'_\infty(u-u')^2 ds'ds\,,$$

showing already that L is a Lyapunov function. Symmetrization and the fact that $\max p_\infty = \sqrt{\kappa_{sev}/(ev)}$ imply

$$\begin{aligned}
\frac{dL}{dt} &= -\frac{\kappa_{sev}}{4}\int_0^\infty\int_0^\infty \big(H(s'\to s)p'_\infty + H(s\to s')p_\infty\big)(u-u')^2 ds'ds \\
&\le -\frac{\sqrt{\kappa_{sev}ev}}{4}\int_0^\infty\int_0^\infty \big(H(s'\to s)+H(s\to s')\big)p'_\infty p_\infty (u-u')^2 ds'ds \\
&= -\frac{\sqrt{\kappa_{sev}ev}}{4}\int_0^\infty\int_0^\infty p'_\infty p_\infty \big(u^2-2uu'+(u')^2\big)^2 ds'ds \\
&= -\sqrt{\kappa_{sev}ev}\,L\,.
\end{aligned}$$

As a consequence of the Gronwall lemma, $L(t)\to 0$ exponentially as $t\to\infty$, implying that $p(\cdot,t)\to p_\infty$ also exponentially in the L^2-space with weight p_∞^{-1}.

How long are the filaments on the average? The expected length in equilibrium is

$$\overline{s} = \int_0^\infty s\,p_\infty(s)ds = \sqrt{\frac{\pi v}{2\kappa_{sev}}}\,.$$

As expected, stronger severing makes them shorter and faster polymerization makes them longer.

Returning to chemotaxis, we introduce friction proportional to the width of the lamellipodium, i.e. to the expected equilibrium length of filaments, i.e. to the square root of the polymerization speed. This gives the model

$$\begin{aligned}
-\kappa_r(\dot{x}_r - v_r) - \mu(x_r - x_l - L) &= 0\,,\\
-\kappa_l(\dot{x}_l + v_l) + \mu(x_r - x_l - L) &= 0\,,
\end{aligned}$$

with $\kappa_{l,r} = \kappa_0\sqrt{v_{l,r}}$. As $t\to\infty$, the velocity of the cell converges to $\frac{\kappa_r v_r - \kappa_l v_l}{\kappa_r+\kappa_l}$, and for the speeds of the actin material relative to the substrate on the right and on the left we have

$$|\dot{x}_r - v_r| \to \frac{\kappa_l}{\kappa_r+\kappa_l}(v_r+v_l)\,,\qquad |\dot{x}_l + v_l| \to \frac{\kappa_r}{\kappa_r+\kappa_l}(v_r+v_l)\,,$$

in qualitative agreement with the experimental results.

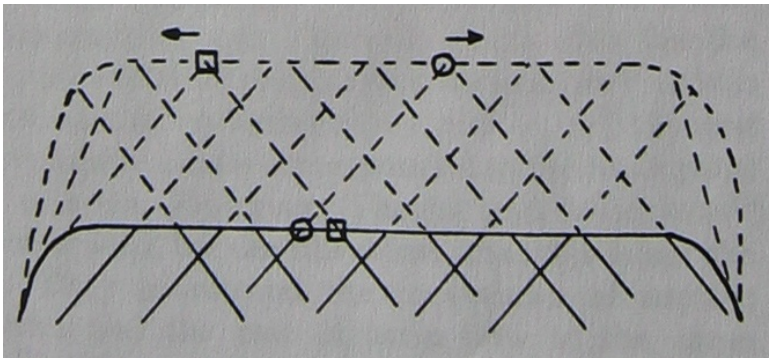

Figure 17: Explanation of lateral flow along the leading edge of the lamellipodium. Source: J. Vic Small.

5.6 Branching, capping, and lateral flow of filament ends

The leading edge is assumed as a rectifiable curve of length L, parametrized by arclength $x \in [0, L]$. We distinguish between two families of filaments, those pointing to the right with number density of ends $u(x,t)$ and those pointing to the left with density $v(x,t)$. By lateral flow the right-pointing filament ends are moved to the right and the left-pointing filament ends to the left. As a simplifying assumption we consider a given constant lateral flow speed $c > 0$ for both families.

The density of Arp2/3 is denoted by $a(x,t)$. It is assumed to be recruited from the cytoplasm to the leading edge with a constant rate c_{rec} with the opposite reaction working towards the equilibrium value a_0. Furthermore Arp2/3 is consumed by branching events, where filament ends of one family create ends of the other with rate constant κ_{br}. Arp2/3 molecules at the leading edge are assumed immobile for simplicity. Finally, the rate constant for the deactivating capping reaction is denoted by κ_{cap}. These assumptions lead to the system

$$\begin{aligned}
\partial_t u + \partial_x(cu) &= \kappa_{\mathrm{br}} \frac{a}{a_0} v - \kappa_{\mathrm{cap}} u \,, \\
\partial_t v - \partial_x(cv) &= \kappa_{\mathrm{br}} \frac{a}{a_0} u - \kappa_{\mathrm{cap}} v \,, \\
\partial_t a &= c_{\mathrm{rec}} \left(1 - \frac{a}{a_0}\right) - \kappa_{\mathrm{br}} \frac{a}{a_0}(u+v) \,.
\end{aligned}$$

We introduce the scaling

$$x \to x\,L, \quad t \to \frac{t}{\kappa_{\rm cap}}, \quad c \to L\,\kappa_{\rm cap} c, \quad (u,v) \to \left(u\frac{c_{\rm rec}}{\kappa_{\rm br}}, v\frac{c_{\rm rec}}{\kappa_{\rm br}}\right), \quad a \to a_0 a,$$

and the dimensionless parameters

$$\alpha := \frac{\kappa_{\rm br}}{\kappa_{\rm cap}}\,, \qquad \varepsilon = \frac{\kappa_{\rm cap} a_0}{c_{\rm rec}}\,,$$

where α, the ratio between the branching and the capping rates, is assumed of moderate size, whereas ε, the ratio between the characteristic time for Arp2/3 and that of the capping and branching processes will be assumed as small. Whereas the first assumption is justified and actually necessary, as our analysis will show, the smallness of ε has, to the knowledge of the author, not been verified experimentally. The nondimensionalized system has the form

$$\begin{aligned} \partial_t u + \partial_x(cu) &= \alpha a v - u\,, \\ \partial_t v - \partial_x(cv) &= \alpha a u - v\,, \\ \varepsilon \partial_t a &= 1 - a(1+u+v)\,. \end{aligned}$$

The last step in the model derivation is to pass to the quasistationary limit $\varepsilon \to 0$ in the equation for a, which is analogous to the derivation of Michaelis-Menten kinetics. Elimination of a from the resulting system gives

$$\begin{aligned} \partial_t u + \partial_x\,(cu) &= \frac{\alpha\, v}{1+u+v} - u\,, \\ \partial_t v - \partial_x\,(cv) &= \frac{\alpha\, u}{1+u+v} - v\,, \end{aligned} \tag{52}$$

for $x \in [0,1]$. Two types of boundary conditions are biologically relevant. In the case of a ring-shaped lamellipodium around the whole cell (see Fig. 18, right) we assume periodic boundary conditions. On the other hand, if we consider only a lamellipodium at the front (see Fig. 18, left), it is reasonable to assume that no left-moving filaments enter from the right and vice versa.

These considerations allow to complement (52) with either Dirichlet or periodic boundary conditions:

$$\text{(DBC)} \quad u(0,t) = 0, \quad v(1,t) = 0, \quad \text{for } t > 0\,, \tag{53}$$

$$\text{(PBC)} \quad u(0,t) = u(1,t), \quad v(0,t) = v(1,t), \quad \text{for } t > 0. \tag{54}$$

To complete the definition of the problem, we pose initial conditions

$$u(x,0) = u_0(x)\,, \quad v(x,0) = v_0(x)\,, \qquad \text{for } x \in [0,1]\,, \tag{55}$$

with given $u_0(x), v_0(x)$, which are assumed to be non-negative and to satisfy the boundary conditions.

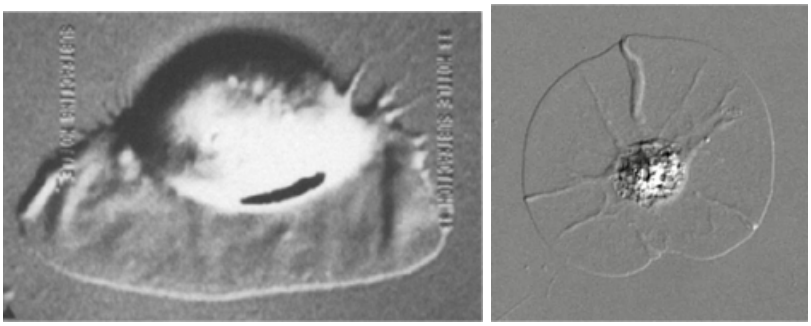

Figure 18: Left: Fish keratocyte with lamellipodium only on one side. Right: Coelocyte with lamellipodium around the cell body.

Position independent solutions for (PBC): We start with some observations for (PBC): If the initial data u_0, v_0 are independent from x, then this property is propagated, and we just have to solve the ODE system

$$\begin{aligned} \frac{du}{dt} &= \frac{\alpha\, v}{1+u+v} - u\,, \\ \frac{dv}{dt} &= \frac{\alpha\, u}{1+u+v} - v\,. \end{aligned} \tag{56}$$

Obviously there is the trivial steady state $(0,0)$ (If there are no filaments initially, there cannot be any branching to create filaments). For $\alpha > 1$ there exists the second nonnegative equilibrium $u_\infty = v_\infty = \frac{\alpha-1}{2}$.

The stability is easily understood, since the problem can be reduced to one ODE for $u+v$:

$$\frac{d}{dt}(u+v) = \frac{(u+v)(\alpha - 1 - (u+v))}{1+(u+v)}$$

This shows the occurrence of a *transcritical bifurcation* (see Fig. 19) at $\alpha = 1$. For $\alpha < 1$ the steady state $u+v=0$ is (globally asymptotically) stable, and for $\alpha > 1$ the nontrivial steady state $u+v = \alpha - 1$ is stable (asymptotically, almost globally).

The analysis of the system can be completed by considering

$$\frac{d}{dt}(u-v) = -(u-v)\left(1 + \frac{\alpha}{1+u+v}\right)\,,$$

which shows that $u-v$ always converges to zero exponentially.

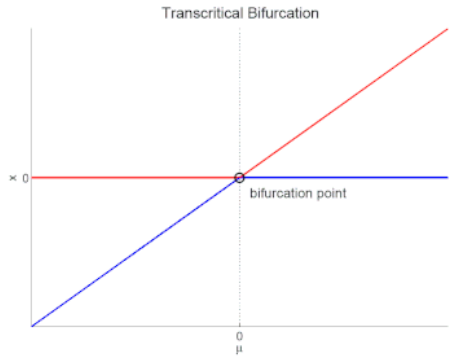

Figure 19: Bifurcation diagram of the transcritical bifurcation. x corresponds to $u+v$ and μ to $\alpha-1$. *Red* means stable, *blue* means unstable.

Convergence to zero for $\alpha < 1$: Some of these results can be transferred to the PDE problem. For example we shall prove that for $\alpha < 1$ all solutions converge to zero. Actually, in this case

$$L(t) = \frac{1}{2}\int_0^1 \left(u(x,t)^2 + v(x,t)^2\right) dx$$

serves as a Lyapunov function:

$$\frac{dL}{dt} \le \int_0^1 \left(\frac{2\alpha uv}{1+u+v} - u^2 - v^2\right) dx < -\int_0^1 (u-v)^2 dx \le 0\,.$$

The first inequality is an equality for (PBC). For (DBC) we have dropped the additional term $-c(u(1,t)^2 + v(0,t)^2)/2 \le 0$. The second inequality is obvious and shows that the Lyapunov function is nonincreasing, but it is not quite good enough. Actually

$$\frac{dL}{dt} \le \int_0^1 \frac{(\alpha-1)(u^2+v^2) - \alpha(u-v)^2 - (u+v)(u^2+v^2)}{1+u+v} dx \le 2(\alpha-1)L\,,$$

implying by the Gronwall lemma exponential decay of u and v in $L^2(0,1)$ as $t \to \infty$.

Transcritical bifurcation for (DBC): A transcritical bifurcation from the trivial steady can only happen for a value of α, where the linearized (around the trivial steady state) stationary problem does not have a unique

solution. For example: The Jacobian

$$\begin{pmatrix} -1 & \alpha \\ \alpha & -1 \end{pmatrix},$$

of the right hand side of (56) at $(u, v) = (0, 0)$ is invertible except at the bifurcation point $\alpha = 1$.

As a first step we rewrite the system (52) in the form

$$\partial_t \begin{pmatrix} u \\ v \end{pmatrix} = \mathcal{L}_\alpha(u, v) - \frac{\alpha(u+v)}{1+u+v} \begin{pmatrix} v \\ u \end{pmatrix}, \tag{57}$$

where

$$\mathcal{L}_\alpha(u, v) := \begin{pmatrix} \mathcal{L}_{\alpha,1}(u, v) \\ \mathcal{L}_{\alpha,2}(u, v) \end{pmatrix} = \begin{pmatrix} \alpha v - u - c\partial_x u \\ \alpha u - v + c\partial_x v \end{pmatrix},$$

denotes the linearization at $(u, v) = (0, 0)$ and the last term in (57) is the quadratic remainder. Without giving a precise functional analytic framework, we assume that the boundary conditions (DBC) are included in the definition of the domain of $\mathcal{L}_\alpha$, i.e.

$$(u, v) \in D(\mathcal{L}_\alpha) \quad \Longrightarrow \quad u(0) = v(1) = 0\,.$$

In the linearized stationary problem $\mathcal{L}_\alpha(u, v) = 0$ we first eliminate v:

$$c\partial_x^2 u = \alpha\partial_x v - \partial_x u = \frac{\alpha}{c}(v - \alpha u) - \partial_x u = \frac{1}{c}(c\partial_x u + u) - \frac{\alpha^2}{c}u - \partial_x u = -\frac{\alpha^2 - 1}{c}u\,,$$

Since we have already shown stability of $(u, v) = (0, 0)$ for $\alpha < 1$, we now assume $\alpha > 1$. With the boundary condition for u this implies

$$u(x) = a\sin(bx)\,,$$

with $b = \sqrt{(\alpha^2 - 1)}/c$ and an arbitrary constant a. This implies

$$v(x) = \frac{a}{\alpha}(\sin(bx) + bc\cos(bx))\,.$$

Since we look for a nontrivial solution, the boundary condition for v implies for the bifurcation point

$$\tan b = -bc\,.$$

The smallest positive solution b_0 of this equation satisfies $\pi/2 < b_0 < \pi$. This gives the bifurcation point

$$\alpha_0 = \sqrt{1 + b_0^2 c^2} = \sqrt{1 + \tan^2 b_0} = -\frac{1}{\cos b_0}\,.$$

Therefore

$$\begin{aligned} v(x) &= \frac{a}{\alpha_0}(\sin(b_0 x) + -\tan b_0 \cos(b_0 x)) = \frac{a}{\alpha_0 \cos b_0}\sin(b_0(x-1)) \\ &= a\sin(b_0(1-x))\,, \end{aligned}$$

and we recall $u(x) = a\sin(b_0 x)$. We deduce that $\mathcal{L}_{\alpha_0}$ has a simple zero eigenvalue, where the eigenspace is spanned by

$$\begin{pmatrix} \tilde{u}(x) \\ \tilde{v}(x) \end{pmatrix} := \begin{pmatrix} \sin(b_0 x) \\ \sin(b_0(1-x)) \end{pmatrix}.$$

As a preparatory step we think about inhomogeneous problems of the form

$$\mathcal{L}_{\alpha_0}(u,v) = \begin{pmatrix} f \\ g \end{pmatrix}. \tag{58}$$

Since the homogeneous equation does not have a unique solution, we expect that the inhomogeneous equation requires a solvability condition for the inhomogeneity. If we introduce the L^2-scalar product

$$\left\langle \begin{pmatrix} u_1 \\ v_1 \end{pmatrix}, \begin{pmatrix} u_2 \\ v_2 \end{pmatrix} \right\rangle := \int_0^1 (u_1 u_2 + v_1 v_2) dx\,,$$

we have, for $(u_1, v_1) \in D(\mathcal{L}_{\alpha_0})$,

$$\begin{aligned} \left\langle \mathcal{L}_{\alpha_0}(u_1,v_1), \begin{pmatrix} u_2 \\ v_2 \end{pmatrix} \right\rangle &= \int_0^1 [(\alpha v_1 - u_1 - c\partial_x u_1)u_2 + (\alpha u_1 - v_1 + c\partial_x v_1)v_2] dx \\ &= \int_0^1 [u_1(\alpha v_2 - u_2 + c\partial_x u_2) + v_1(\alpha u_2 - v_2 - c\partial_x v_2)] dx\,, \end{aligned}$$

by integration by parts and with the assumption $u_2(1) = v_2(0) = 0$. Since the right hand side should be equal to $\langle (u_1,v_1), \mathcal{L}^*_{\alpha_0}(u_2,v_2)\rangle$, this gives the adjoint operator

$$\mathcal{L}^*_{\alpha_0}(u,v) = \begin{pmatrix} \mathcal{L}_{\alpha,2}(v,u) \\ \mathcal{L}_{\alpha,1}(v,u) \end{pmatrix},$$

and therefore $\mathcal{L}^*_{\alpha_0}(\tilde{v},\tilde{u}) = 0$. If $\mathcal{L}_{\alpha_0}$ were a matrix then $(\tilde{v},\tilde{u})$ would be called a left eigenvector for the eigenvalue zero. The solvability condition for (58) is obtained by taking the scalar product with $(\tilde{v},\tilde{u})$:

$$\left\langle \begin{pmatrix} f \\ g \end{pmatrix}, \begin{pmatrix} \tilde{v} \\ \tilde{u} \end{pmatrix} \right\rangle = \int_0^1 (f(x)\sin(b_0(1-x)) + g(x)\sin(b_0 x)) dx = 0\,.$$

Now we are ready for the bifurcation analysis. We look at the situation close to the bifurcation point and set $\alpha = \alpha_0 + \varepsilon$ with $|\varepsilon| \ll 1$. We also look for solutions close to the trivial solution. Furthermore we expect variations on the slow time scale $\tau = |\varepsilon| t$ (if this is not obvious at the moment, it will become clear below) and make the ansatz

$$u(x,t) = \varepsilon u_1(x,\tau) + O(\varepsilon^2)\,, \qquad v(x,t) = \varepsilon v_1(x,\tau) + O(\varepsilon^2)\,.$$

which will be substituted in (57),

$$\partial_t \begin{pmatrix} u \\ v \end{pmatrix} = \mathcal{L}_{\alpha_0}(u,v) + \varepsilon \begin{pmatrix} v \\ u \end{pmatrix} - \frac{(\alpha_0+\varepsilon)(u+v)}{1+u+v} \begin{pmatrix} v \\ u \end{pmatrix},$$

giving

$$|\varepsilon| \partial_\tau \begin{pmatrix} u_1 \\ v_1 \end{pmatrix} = \mathcal{L}_{\alpha_0}(u_1,v_1) + \varepsilon \begin{pmatrix} v_1 \\ u_1 \end{pmatrix} - \varepsilon\alpha_0 (u_1+v_1) \begin{pmatrix} v_1 \\ u_1 \end{pmatrix} + O(\varepsilon^2)\,. \qquad (59)$$

The limit $\varepsilon \to 0$ implies

$$\begin{pmatrix} u_1(x,\tau) \\ v_1(x,\tau) \end{pmatrix} = a(\tau) \begin{pmatrix} \tilde{u}(x) \\ \tilde{v}(x) \end{pmatrix},$$

with an as yet unknown $a(\tau)$. An equation for a is obtained by seeing (59) as an equation of the form (58), writing the solvability condition, and passing to $\varepsilon \to 0$:

$$\sigma\kappa_0 \frac{da}{d\tau} = \kappa_1 a - \kappa_2 a^2\,,$$

with

$$\sigma = \mathrm{sign}(\varepsilon)\,, \qquad \kappa_0 = 2\int_0^1 \tilde{u}\tilde{v}\,dx\,, \qquad \kappa_1 = \int_0^1 (\tilde{u}^2+\tilde{v}^2)dx\,,$$

$$\kappa_2 = \alpha_0 \int_0^1 (\tilde{u}+\tilde{v})(\tilde{u}^2+\tilde{v}^2)dx\,.$$

Since $\kappa_0, \kappa_1, \kappa_2 > 0$, $a = 0$ is stable for $\varepsilon < 0$, and $a = \kappa_1/\kappa_2 > 0$ is stable for $\varepsilon > 0$.

The conclusion is that there is a transcritical bifurcation at $\alpha = \alpha_0$ with the steady state $(u,v) = (0,0)$ stable for $\alpha < \alpha_0$, and the steady state

$$(\alpha - \alpha_0)\frac{\kappa_1}{\kappa_2} \begin{pmatrix} \sin(b_0 x) \\ \sin(b_0(1-x)) \end{pmatrix} + O((\alpha-\alpha_0)^2)$$

stable for $\alpha > \alpha_0$. This result can be made rigorous (for more details see [10]). Fig. 20 shows a numerically computed steady state far from the bifurcation. The qualitative behaviour of the bifurcating solution can still be recognized.

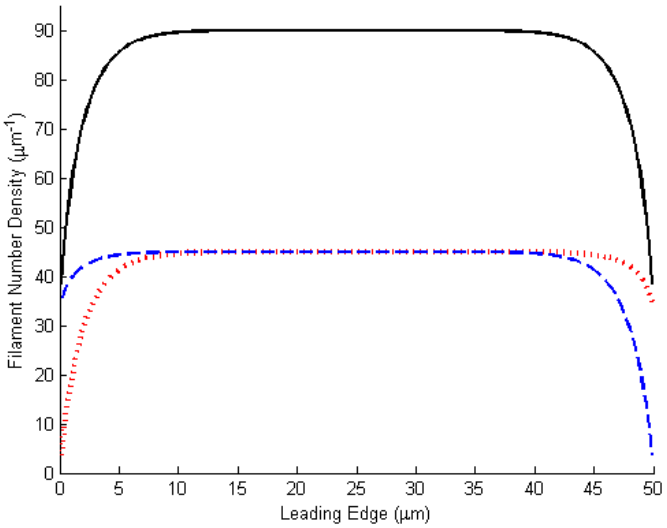

Figure 20: Steady state of (52) with (DBC) far from the transcritical bifurcation. u in red, v in blue, $u+v$ in black. Source: [10].

5.7 Bending of actin filaments

Actin filaments have a thickness of about 7nm, they can have a length of several μm, and they have a helical structure with a pitch of about 37nm (see Fig. 21). In this section their bending properties will be discussed. In equilibrium, i.e. with no forces acting on them, they are straight. Because of their large *aspect ratio* (length/thickness) we shall describe bent filaments as curves. We have in mind experiments as shown in Fig. 21, where filaments are lying on a flat substrate, whence the curves are subsets of $\mathbb{R}^2$. Since stretching forces on filaments are typically weak, we assume *inextensibility*, which means that filaments have a fixed length. Even stronger: the length between two arbitrary material points does not change. Therefore, if a moving filament $F(t)$ of length L is parametrized by arclength $s \in [0, L]$,

$$F(t) = \{z(s,t) : 0 \le s \le L\} \subset \mathbb{R}^2 \qquad \text{where } |z'(s,t)| = 1\,, \quad 0 \le s \le L\,,\, t \ge 0\,,$$

then the arclength s can also be interpreted as a *Lagrangian* (i.e. material) coordinate, which means that for fixed s the map $t \mapsto z(s,t)$ describes the path of a material particle. As an example consider the circle C_R with radius R and length $2R\pi$:

$$C_R = \{z_R(s) = R(\cos(s/R), \sin(s/R)) : 0 \le s < 2R\pi\}$$

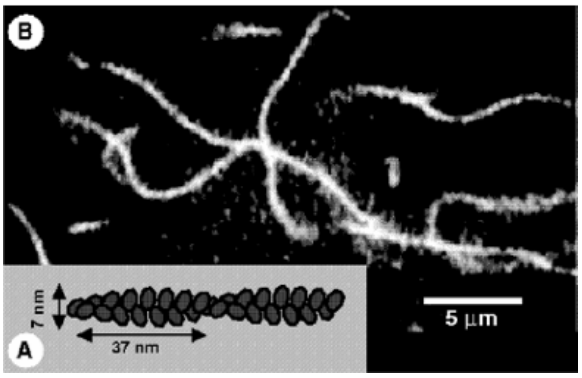

Figure 21: Bending of actin filaments

Note that

$$z_R''(s) = -\frac{1}{R}(\cos(s/R), \sin(s/R)) \qquad \text{and} \qquad |z_R''(s)| = \frac{1}{R}\,.$$

The inverse of the radius is called the *curvature*. For general curves, the local curvature is given by $|z''(s)|$ and it can be interpreted as the inverse of the radius of the *osculating* (i.e. 'kissing') *circle* (the best local approximation of the curve by a circle).

We postulate that the potential energy for bending takes the form of the *Kirchhoff bending energy*

$$\mathcal{E}^B[z] := \frac{\mu^B}{2}\int_0^L |z''(s)|^2 ds\,,$$

the square of the L^2-norm of the curvature, with $\mu^B > 0$. Note that the state space is given by the set of all functions $z : [0, L] \to \mathbb{R}^2$, smooth enough for the bending energy to exist and satisfying the constraint $|z'(s)| = 1$. Note that this is not a linear space. We shall interpret it as a manifold in $L^2(0, L)^2$. We want to describe an experiment, where a bent filament is put on the flat substrate where it moves against the resistance of friction between the filament and the substrate with friction constant κ. This puts us in the situation described at the end of Section 5.2. We define the set

$$Z = \{z \in C^1([0, L]) : |z'| = 1 \text{ on } [0, L]\}\,,$$

and the dynamics of the filament $F(t)$ by (compare to (49)) $z(\cdot, t) = \lim_{h\to 0} z_h(\cdot, t)$ with

$$z_h(\cdot, t) = \operatorname{argmin}_{y\in Z}\left(\frac{\kappa}{2h}\|y - z_h(\cdot, t-h)\|^2_{L^2(0,L)^2} + \mathcal{E}^B[y]\right)\,.$$

This is a constrained minimization problem, which can be solved by introducing the Lagrangian

$$\mathcal{L}^B[y,\lambda] := \frac{\kappa}{2h}\|y - z_h(\cdot,t-h)\|^2_{L^2(0,L)^2} + \mathcal{E}^B[y] + \frac{1}{2}\int_0^L \lambda(s,t)(|y'(s)|^2 - 1)ds\,,$$

with the Lagrange multipliers $\lambda(s,t)$. Note that, in order to produce a smooth Lagrangian, we have replaced the constraint by $|y'(s)|^2 = 1$. Now $(z_h(\cdot,t)),\lambda)$ is an unconstrained stationary point of the Lagrangian, implying $\nabla\mathcal{L}^B[z_h(\cdot,t),\lambda] = 0$, where the gradient denotes the L^2-representation of the Fréchet derivative. The gradient can be computed by computing directional (Gâteaux) derivatives:

$$\langle \nabla E(z), y\rangle = \frac{d}{d\delta}E(z+\delta y)\mid_{\delta=0}\ .$$

We compute the gradients of the three terms in the Lagrangian separately. The first term, evaluated at $z_h(\cdot,t)+\delta y$, is given by

$$\frac{\kappa}{2h}\int_0^L |z_h(s,t) + \delta y(s) - z_h(s,t-h)|^2\,ds\,.$$

The derivative with respect to δ, evaluated at $\delta = 0$, gives

$$\kappa\int_0^L \frac{z_h(s,t) - z_h(s,t-h)}{h}\cdot y(s)ds = \left\langle \kappa\frac{z_h(\cdot,t) - z_h(\cdot,t-h)}{h}, y\right\rangle\ . \quad (60)$$

For the second term we have

$$\mathcal{E}^B[z_h(\cdot,t)+\delta y] = \frac{\mu^B}{2}\int_0^L |z_h''(s,t) + \delta y''(s)|^2 ds\,,$$

and the derivative

$$\mu^B\int_0^L z_h''(s,t)\cdot y''(s)ds\,.$$

In order to obtain the desired form (scalar product with a factor y), we need to integrate by parts twice:

$$\begin{aligned}\mu^B\int_0^L z_h''\cdot y''ds &= \mu^B z_h''\cdot y'\mid_0^L - \mu^B\int_0^L z_h'''\cdot y'ds\\ &= \mu^B(z_h''\cdot y' - z_h'''\cdot y)\mid_0^L + \mu^B\int_0^L z_h^{(4)}\cdot y\,ds \quad (61)\end{aligned}$$

Now the last term is in the desired form, but we also have to deal with boundary terms. The same happens for the third term. Evaluation at $z_h(\cdot,t)+\delta y$:

$$\frac{1}{2}\int_0^L \lambda(s)(|z_h'(s,t)+\delta y'(s)|^2-1)ds\,.$$

Derivative:

$$\int_0^L \lambda z_h'\cdot y'ds = \lambda z_h'\cdot y\,|_0^L - \int_0^L (\lambda z_h')'\cdot y\,ds\,. \tag{62}$$

The combination of (60)–(62) implies

$$\int_0^L \left(\kappa\frac{z_h(s,t)-z_h(s,t-h)}{h}+\mu^B z_h^{(4)}(s,t)-(\lambda(s,t)z_h'(s,t))'\right)\cdot y(s)ds$$
$$+(\mu^B z_h''\cdot y'+(\lambda z_h'-\mu^B z_h''')\cdot y)\,|_0^L=0\,,$$

for every y (without going into detail of what this means precisely). It is a standard argument of the calculus of variations to first use test functions y such that y and y' vanish at the boundary points. With $h\to 0$ this implies the system of partial differential equations

$$\kappa\,\partial_t z+\mu^B\partial_s^4 z-\partial_s(\lambda\partial_s z)=0\,.$$

Now we use test functions such that three of the four values $y(0),y(L),y'(0),y'(L)$ vanish. This implies the boundary conditions

$$\partial_s^2 z=\mu^B\partial_s^3 z-\lambda\partial_s z=0\qquad\text{at } s=0,L\,.$$

Finally, we still have to satisfy the constraint

$$|\partial_s z|=1\,,$$

which can be seen as an equation for the additional unknown λ.

Recalling (50), we expect the bending energy to be nonincreasing along solutions:

$$\begin{aligned}\frac{d}{dt}\mathcal{E}^B[z] &= \mu^B\int_0^L \partial_s^2 z\cdot\partial_t\partial_s^2 z\,ds=-\mu^B\int_0^L\partial_s^3 z\cdot\partial_t\partial_s z\,ds\\ &= -\mu^B\partial_s^3 z\cdot\partial_t z\,|_0^L+\mu^B\int_0^L\partial_s^4 z\cdot\partial_t z\,ds\,,\end{aligned}$$

where in the first integration by parts the boundary terms vanish because of the boundary conditions. We shall also need

$$\int_0^L \partial_s(\lambda\partial_s z)\cdot\partial_t z\,ds = \lambda\partial_s z\cdot\partial_t z\mid_0^L - \int_0^L \lambda\partial_s z\cdot\partial_t\partial_s z\,ds = \lambda\partial_s z\cdot\partial_t z\mid_0^L,$$

where the second equality follows from the derivative of the constraint $|\partial_s z|^2 = 1$ with respect to t. With this identity, we obtain

$$\begin{aligned}\frac{d}{dt}\mathcal{E}^B[z] &= (\lambda\partial_s z - \mu^B\partial_s^3 z)\cdot\partial_t z\mid_0^L + \int_0^L (\mu^B\partial_s^4 z - \partial_s(\lambda\partial_s z))\cdot\partial_t z\,ds \\ &= -\frac{1}{\kappa}\int_0^L \left|\mu^B\partial_s^4 z - \partial_s(\lambda\partial_s z)\right|^2 ds \le 0\,.\end{aligned}$$

Since $\mathcal{E}^B$ is bounded from below, we expect that the right hand side tends to zero. If we assume convergence of the solution to a steady state, i.e. $z(s,t)\to z_\infty(s)$, $\lambda(s,t)\to\lambda_\infty(s)$ as $t\to\infty$, we expect $\mu^B\partial_s^4 z_\infty - \partial_s(\lambda_\infty\partial_s z_\infty) = 0$, implying

$$\mu^B\partial_s^3 z_\infty - \lambda_\infty\partial_s z_\infty = 0\,, \tag{63}$$

because of the boundary conditions. Since $\partial_s z_\infty$ has length one, it can be written as $\partial_s z_\infty = (\cos\varphi, \sin\varphi)$. Since then $\partial_s^2 z_\infty = \partial_s\varphi(-\sin\varphi, \cos\varphi)$, the boundary condition $\partial_s\varphi = 0$ for $s = 0, L$ follows. The equation (63) becomes

$$\mu^B\partial_s^2\varphi\begin{pmatrix}-\sin\varphi\\ \cos\varphi\end{pmatrix} - (\mu^B(\partial_s\varphi)^2 + \lambda_\infty)\begin{pmatrix}\cos\varphi\\ \sin\varphi\end{pmatrix} = 0\,.$$

Since the left hand side is a linear combination of orthogonal vectors, both coefficients vanish. From $\partial_s^2\varphi = 0$ and the boundary condition we obtain $\varphi = \text{const}$ and $\lambda_\infty = 0$. This implies that the equilibrium is a straight line segment with the parametrization

$$z_\infty(s) = \overline{z} + \left(s - \frac{L}{2}\right)\begin{pmatrix}\cos\varphi\\ \sin\varphi\end{pmatrix}, \qquad 0\le s\le L\,.$$

What can be said about the values of $\overline{z}$ and φ? From the differential equations and the boundary conditions we conclude that the center of mass does not move:

$$\frac{d}{dt}\int_0^L z(s,t)ds = 0\,.$$

If the initial position is given by $z(s,0) = z_0(s)$, then we have

$$\overline{z} = \frac{1}{L}\int_0^L z_0 ds\,.$$

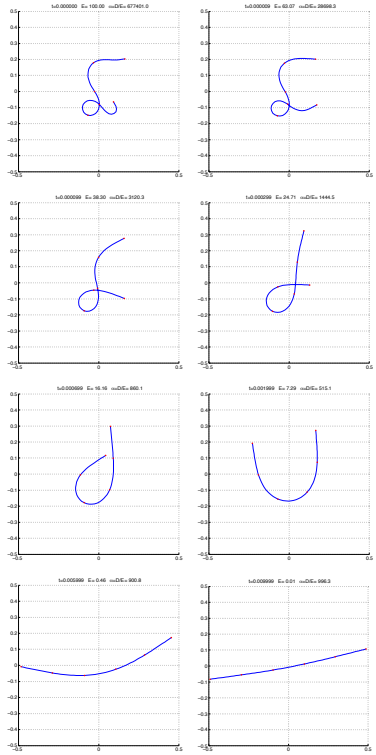

Figure 22: Snapshots of a numerical simulation of curve straightening. Try to predict the final direction (bottom right) from looking only at the initial deformation (top left). Source: [13].

We are not aware of another conservation law and therefore also not of a formula for the computation of φ. However, the convergence result as $t \to \infty$ including the existence of φ can be proven rigorously [13]. As an illustration see the numerical simulation results in Fig. 22.

5.8 The Filament Based Lamellipodium Model (FBLM)

The FBLM is a two-dimensional continuum model for the dynamics of the lamellipodium. It uses most of the ideas introduced in the earlier sections of this chapter as building blocks. The idea is not so much to have one perfect model, but a modeling framework for testing the relative importance of various phenomena.

The cartoon in Fig. 13 of the lamellipodium structure has been veri-

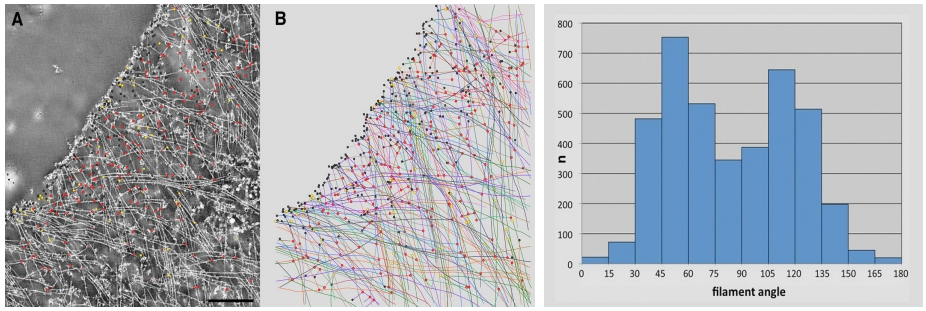

Figure 23: Electron microscopy and tomography of a piece of lamellipodium. Left: 2D projection of a tomogram. Center: Identification of the filament network. Right: Distribution of filament angles relative to the leading edge. Source: [20].

fied by electron microscopy and subsequent tomography (see Fig. 23). This procedure produces three-dimensional pictures of the actin filament network with a resolution of a few nm, such that individual filaments can be identified. As soon as this has been carried out (either by automatic or manual image processing) statistical information about the network properties can be computed easily. Here we concentrate only on one property deduced from a projection of the three-dimensional network to the flat substrate. The angle distribution of the filaments, depicted in Fig. 23, shows two significant peaks, roughly symmetric with respect to the direction of the leading edge and roughly 70 degrees apart. Therefore the cartoon (Fig. 13), splitting the filaments into two groups, can be seen as an idealization, which we shall adopt for the FBLM. The angle of approximately 70 degrees can be seen as a property of the Arp2/3 complex. It can be observed in in-vitro experiments as the force free equilibrium angle of branches.

Two filament families: Fig. 24 provides a graphical overview of the FBLM. We shall refer to it when introducing the details. As mentioned above, the filaments are split into two groups, called the plus-family (right-going) and the minus-family (left-going). Within one family, filaments are assumed as locally parallel without any crossings. On the other hand, when a plus-filament crosses a minus-filament, the crossing is always assumed as transversal, i.e. not tangential. Both families are continua of filaments, parametrized by

$$F^{\pm}(\alpha, s, t)\,, \quad (\alpha, s) \in B^{\pm}(t) := \{(\alpha, s) \in \mathbb{T}^1 \times \mathbb{R} : \, 0 \le s \le L^{\pm}(\alpha, t)\}\,, \quad t \ge 0\,,$$

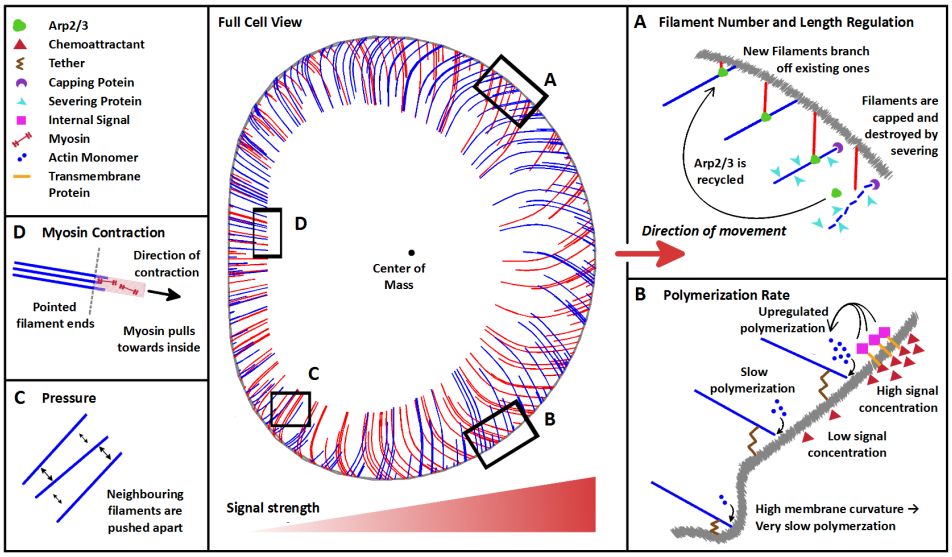

Figure 24: Graphical overview of the FBLM. Source: [8].

where α is a *filament label.* Since we consider a lamellipodium around the cell, it is a periodic variable in the one-dimensional torus $\mathbb{T}^1$, represented by the interval $[0, 2\pi)$. The coordinate s denotes *arc length* along the filament, i.e.

$$|\partial_s F^{\pm}| = 1\,. \tag{64}$$

It is increasing inwards, i.e. $s = 0$ corresponds to the barbed end of the filament, assumed to be always in contact with the leading edge (the outer boundary) of the lamellipodium, which has to be the same for both families, of course, leading to the constraint

$$\{F^{+}(\alpha, 0, t) : \alpha \in \mathbb{T}^1\} = \{F^{-}(\alpha, 0, t) : \alpha \in \mathbb{T}^1\}\,, \qquad t \geq 0\,. \tag{65}$$

The *maximal length* of the filament with label α at time t is denoted by $L^{\pm}(\alpha, t)$. 'Maximal length', since in this continuum description $F^{\pm}(\alpha, \cdot, t)$ stands for an ensemble of filaments of varying lengths.

The filament density: The length distribution is described by the *density*

$$\eta^{\pm}(\alpha, s, t) > 0\,.$$

Its leading edge values $\eta^{\pm}(\alpha, 0, t)$ give the number density of barbed ends along the leading edge. The map $s \mapsto \eta^{\pm}(\alpha, s, t)$ is nonincreasing, indicating the fact that all barbed ends touch the leading edge. The ratio $\eta^{\pm}(\alpha, s, t)/\eta^{\pm}(\alpha, 0, t) \in (0, 1]$ gives the proportion of filaments with length at least s. The picture in the center of Fig. 24 has been produced by stochastic sampling from simulation data for $F^{\pm}$ and $\eta^{\pm}$. Another interpretation of $\eta^{\pm}$ is that of a *filament length density* (with respect to (α, s)).

Lamellipodium area – filament crossings: The set $\mathcal{L}^{\pm}(t) := F^{\pm}(B^{\pm}(t), t)$ is the area covered by the $\pm$-family. The two are not necessarily the same. The lamellipodium area at time t is given by $\mathcal{L}(t) := \mathcal{L}^{+}(t) \cup \mathcal{L}^{-}(t)$. We denote laboratory (Eulerian) coordinates by $\mathbf{x} \in \mathbb{R}^2$. Then the transformation from (α, s) to Eulerian coordinates is given by $\mathbf{x} = F^{\pm}(\alpha, s, t)$, and the area element satisfies

$$d\mathbf{x} = \left|\det\left(\partial_\alpha F^{\pm}, \partial_s F^{\pm}\right)\right| d(\alpha, s) = \left|\left(\partial_\alpha F^{\pm}\right)^{\perp} \cdot \partial_s F^{\pm}\right| d(\alpha, s)\,,$$

where we have used the convention $(a, b)^{\perp} = (-b, a)$. At this point we decide about the orientation of the leading edge curve, which we choose as counter-clockwise. This implies that $(\partial_\alpha F^{\pm})^{\perp}$ is an inward normal and

$$d\mathbf{x} = \left(\partial_\alpha F^{\pm}\right)^{\perp} \cdot \partial_s F^{\pm}\, d(\alpha, s)\,.$$

The filament length density $\varrho^{\pm}$ with respect to Eulerian coordinates has to satisfy $\varrho^{\pm} d\mathbf{x} = \eta^{\pm} d(\alpha, s)$. So it is given by

$$\varrho^{\pm} = \frac{\eta^{\pm}}{(\partial_\alpha F^{\pm})^{\perp} \cdot \partial_s F^{\pm}}\,. \tag{66}$$

Crossings of filaments occur in $\mathcal{C}(t) := \mathcal{L}^{+}(t) \cap \mathcal{L}^{-}(t)$. The correspondingly reduced domains $B^{\pm}_{\mathcal{C}}(t)$ are determined such that $F^{\pm}(B^{\pm}_{\mathcal{C}}(t), t) = \mathcal{C}(t)$. We expect that both families provide simple coverings of $\mathcal{C}(t)$, which implies the existence of maps $\psi^{\pm} : B^{\mp}_{\mathcal{C}}(t) \to B^{\pm}_{\mathcal{C}}(t)$ such that

$$F^{\mp} = F^{\pm} \circ \psi^{\pm}\,.$$

Polymerization: We allow for variable *polymerization speed* $v^{\pm}(\alpha, t)$. This means that actin monomers move away from the leading edge with this speed. Therefore s is not a Lagrangian variable, but

$$\sigma = s - \int_0^t v^{\pm}(\alpha, \tau) d\tau\,. \tag{67}$$

The *material derivative* (time derivative for fixed σ) is then given by

$$D_t^{\pm} := \partial_t + \frac{\partial s}{\partial t}\partial_s = \partial_t + v^{\pm}\partial_s \,. \tag{68}$$

The velocity of monomers relative to the substrate is $D_t^{\pm}F^{\pm}$.

The model for the filament density: For modeling the densities η^+ and η^-, we shall combine ideas from Sections 5.5 and 5.6. For the variable x of Section 5.6 we have

$$x = X^{\pm}(\alpha, t) := \int_0^{\alpha} |\partial_\alpha F^{\pm}(\alpha', 0, t)| d\alpha' \,. \tag{69}$$

With the notation from Section 5.6 the requirement

$$u\, dx = \eta^+(s=0) d\alpha$$

for the plus-family implies

$$\eta^+(\alpha, 0, t) = |\partial_\alpha F^+(\alpha, 0, t)| u(X^+(\alpha, t), t) \,.$$

The derivative with respect to t gives

$$\begin{aligned}
\partial_t \eta^+(s=0) &= \partial_t |\partial_\alpha F^+(s=0)| u + |\partial_\alpha F^+(s=0)| \left(\partial_t u + \partial_t X^+ \partial_x u\right) \\
&= |\partial_\alpha F^+(s=0)| \left(\partial_t u + \partial_t X^+ \partial_x u + \frac{\partial_\alpha \partial_t X^+}{\partial_\alpha x} u\right) \\
&= |\partial_\alpha F^+(s=0)| \left(\partial_t u + \partial_t X^+ \partial_x u + \partial_x \partial_t X^+ u\right) \\
&= |\partial_\alpha F^+(s=0)| \left(\partial_t u + \partial_x \left(\partial_t X^+ u\right)\right)
\end{aligned}$$

Comparison with (52) supports that $\partial_t X^+$ can be interpreted as the lateral flow velocity c. An analogous computation holds for the minus-family. Introducing

$$u^+(\alpha, t) = u(X^+(\alpha, t), t) \,, \qquad u^-(\alpha, t) = v(X^-(\alpha, t), t) \,,$$

another comparison with (52) motivates the model

$$\partial_t \eta^{\pm}(s=0) = |\partial_\alpha F^{\pm}(s=0)| \left(\frac{\beta u^{\mp} \circ \psi^{\mp}(s=0)}{1 + u^{\pm} + u^{\mp} \circ \psi^{\mp}(s=0)} - u^{\pm}\right) , \tag{70}$$

where we have used β for the ratio between the branching rate and the capping rate, since α is needed otherwise. Because of the occurrence of the

transformation $\psi^{\mp}$, which makes sure that quantities are evaluated at the same positions, this is not just a system of ODEs. Actually it should not, since it is expected to be in a sense equivalent to (52).

Now we come to the s-dependence of $\eta^{\pm}$ and recall that we interpret $\frac{\eta^{\pm}(\alpha,s,t)}{\eta^{\pm}(\alpha,0,t)}$ as the proportion of filaments with length at least s. In terms of the stochastic model of Section 5.5 it has the meaning of a *cumulative distribution function*, and the relation to the probability density p for the length distribution of filaments is given by

$$\frac{\eta^{\pm}}{\eta^{\pm}(s=0)} = \int_s^{\infty} p(s')ds' \,.$$

For simplicity we assume that the processes regulating the length distribution are fast and therefore always in equilibrium, given by (51), leading to the model

$$\eta^{\pm}(\alpha,s,t) = \eta^{\pm}(\alpha,0,t) \exp\left(-\frac{\kappa_{sev}s^2}{2v^{\pm}(\alpha,t)}\right) , \tag{71}$$

with $\eta^{\pm}(s=0)$ determined by (70), with a constant severing rate κ_{sev}, but with the filament- and time-dependent polymerization rate introduced above. Finally, the lamellipodium region is defined by asking the density to be above a threshold value η_{min}, i.e. we define the maximal length by

$$\eta^{\pm}(\alpha, L^{\pm}(\alpha,t),t) = \eta_{min} \,. \tag{72}$$

The potential energy: The model for the filament movement will be of the form of a generalized gradient flow (see Sections 5.2 and 5.7). The potential energy consists of several parts. The first one is the bending energy, which we know already from Section 5.7:

$$\mathcal{E}^B(t)[F^{\pm}] = \frac{\mu^B}{2} \int_{B^{\pm}(t)} |\partial_s^2 F^{\pm}|^2 \eta^{\pm} d(\alpha,s) \,. \tag{73}$$

The only difference is that the density $\eta^{\pm}$ appears as a weight. The consequence is that, away from the leading edge, where we have less filaments, they are easier to bend. Note also that there is no coupling between different values of α, i.e. the bending energy is not influenced by neighboring filaments.

The second is the elastic energy in branches turned away from the equilibrium angle. For this purpose we need the set of all crossing filament

pairs

$$A_{\mathcal{C}}(t) = \{(\alpha^+,\alpha^-)\in\mathbb{T}^1\times\mathbb{T}^1 : \exists s^\pm = S^\pm(\alpha^+,\alpha^-,t) : F^-(\alpha^-,s^-,t) = F^+(\alpha^+,s^+,t)\}. \tag{74}$$

Note that $s^\pm = S^\pm(\alpha^+,\alpha^-,t)$ is equivalent to $(\alpha^+,s^+) = \psi^+(\alpha^-,s^-)$ and to $(\alpha^-,s^-) = \psi^-(\alpha^+,s^+)$. Now the potential energy in twisted cross-links is defined to be

$$\mathcal{E}^T(t)[F^+,F^-] = \frac{\mu^T}{2}\int_{A_{\mathcal{C}}(t)}(\varphi-\varphi_0)^2\eta^+\eta^- d(\alpha^+,\alpha^-)\,, \tag{75}$$

where $\eta^\pm = \eta^\pm(\alpha^\pm, S^\pm(\alpha^+,\alpha^-,t),t)$, the angle $\varphi\in(0,\pi)$ between crossing filaments is given by

$$\cos\varphi(\alpha^+,\alpha^-,t) = \partial_s F^+(\alpha^+,S^+(\alpha^+,\alpha^-,t),t)\cdot\partial_s F^-(\alpha^-,S^-(\alpha^+,\alpha^-,t),t)\,,$$

and its equilibrium value is φ_0.

For the stability of the model it would be good to have a mechanism which keeps parallel filaments apart from each other. Actually there is a physical argument for such a mechanism. It has been shown that actin filaments usually carry negative electric charges. This provides a repulsive *Coulomb force.*

Digression: Coulomb forces – continuum description: The *Coulomb law* states that the size of the force between two electrical point charges q_1, q_2 located at $x_1, x_2\in\mathbb{R}^3$ is given by

$$\frac{|q_1q_2|}{|x_1-x_2|^2}\,.$$

The force has the direction x_1-x_2. It is repulsive, if the charges have the same sign, i.e. $q_1q_2>0$, and it is attractive otherwise. The forces exerted on a charge by more than one other charges have to be added. Now consider a system of N indistinguishable particles, i.e. they all have the same charge q and the same mass m. The movement of their positions $x_1(t),\dots,x_N(t)$ is determined by Coulomb forces, but we also include friction with friction coefficient κ. Then Newton's law (force = mass×acceleration) implies the ODE system

$$m\ddot{x}_i = \sum_{j\neq i}\frac{q^2(x_i-x_j)}{|x_i-x_j|^3} - \kappa\dot{x}_i\,,\qquad i=1,\dots,N\,.$$

Like almost always in biology we make the assumption to be in the *friction dominated regime,* meaning that the terms on the right hand side are much bigger than

the acceleration term, which we therefore neglect (We have already done that before in Sections 5.2 and 5.7). We also produce a factor $\frac{1}{N}$ by changing the time scale:

$$\kappa \dot{x}_i = \frac{1}{N} \sum_{j \neq i} \frac{q^2 (x_i - x_j)}{|x_i - x_j|^3} \,, \qquad i = 1, \ldots, N \,. \tag{76}$$

We note that this is a gradient flow with the potential energy

$$E^C[x_1, \ldots, x_N] = \frac{1}{N} \sum_{i,j:\, i<j} \frac{q^2}{|x_i - x_j|} \,, \qquad \text{i.e.} \quad \kappa \dot{x}_i = -\nabla_{x_i} E^C[x_1, \ldots, x_N] \,, \tag{77}$$

since

$$\nabla \frac{1}{|x|} = -\frac{x}{|x|^3} \,.$$

A bridge from such a description by point particles to a continuum description by densities is provided by the *empirical measure*

$$\varrho(x,t) = \frac{1}{N} \sum_i \delta(x - x_i(t)) \,,$$

with the Delta-distribution δ, formally satisfying

$$\int_{\mathbb{R}^3} \delta(x - x_0) u(x) dx = u(x_0) \,, \qquad x_0 \in \mathbb{R}^3 \,, \quad u \in C(\mathbb{R}^3) \,.$$

Now (76) can be written as

$$\kappa \dot{x}_i = -\nabla_x \Phi(x_i, t) \,, \tag{78}$$

with the *electrostatic potential*

$$\Phi(x,t) = \int_{y \neq x} \frac{q^2 \varrho(y,t)}{|x - y|} dy \,.$$

The empirical measure ϱ can be seen as a distribution on $\mathbb{R}^4$, and for a test function $u \in C_0^\infty(\mathbb{R}^4)$ (smooth with compact support), we can define distributional derivatives of ϱ by formal integration by parts, such as

$$\begin{aligned}
&\int_{\mathbb{R}^4} u \partial_t \varrho \, dx \, dt = -\int_{\mathbb{R}^4} \varrho \partial_t u \, dx \, dt = -\frac{1}{N} \sum_i \int_{\mathbb{R}} \partial_t u(x_i(t), t) dt \\
&= -\frac{1}{N} \sum_i \int_{\mathbb{R}} \left(\frac{d}{dt} u(x_i(t), t) - \dot{x}_i(t) \cdot \nabla_x u(x_i(t), t) \right) dt \\
&= \frac{1}{N} \sum_i \int_{\mathbb{R}} \dot{x}_i(t) \cdot \nabla_x u(x_i(t), t) dt \,.
\end{aligned}$$

The last equality is due to the fact that u has compact support. Motivated by this result, we multiply (78) by $\frac{1}{N}\nabla_x u(x_i(t),t)$, sum over i, and integrate with respect to t:

$$\kappa \int_{\mathbb{R}^4} u\partial_t \varrho \, dx \, dt = -\int_{\mathbb{R}^4} \varrho \nabla_x \Phi \cdot \nabla_x u \, dx \, dt = \int_{\mathbb{R}^4} u \nabla_x \cdot (\varrho \nabla_x \Phi) dx \, dt \, .$$

This shows that the empirical measure is a distributional solution of

$$\kappa \partial_t \varrho = \nabla_x \cdot (\varrho \nabla_x \Phi) \, , \qquad \Phi(x,t) = \int_{y \neq x} \frac{q^2 \varrho(y,t)}{|x-y|} dy \tag{79}$$

The step from particle to continuum description is just to look for solutions ϱ, which are not only measures, but functions. The PDE experts know that $\frac{-1}{2\pi|x|}$ is the fundamental solution of the Laplace operator in $\mathbb{R}^3$, and therefore the *Poisson equation*

$$\Delta_x \Phi = -2\pi q^2 \varrho$$

holds, a fact which in physics is called the *Gauß law of electrodynamics.* Note that it is just the Coulomb law and a bit of mathematics.

For charged particles moving in an environment at positive temperature it is reasonable to expect also diffusion effects, and therefore (79) is extended to the *drift-diffusion model*

$$\kappa \partial_t \varrho = \nabla_x \cdot (D \nabla_x \varrho + \varrho \nabla_x \Phi) \tag{80}$$

where the *diffusivity* D is typically proportional to the temperature. At this point we definitely leave the particle description, since we expect the parabolic drift-diffusion equation to only have smooth solutions.

The formula (77) motivates the definition of the potential energy functional

$$\begin{aligned} E^C[\varrho] &:= \int_{\mathbb{R}^3 \times \mathbb{R}^3} \frac{q^2 \varrho(x,t) \varrho(y,t)}{|x-y|} \, dx \, dy = \int_{\mathbb{R}^3} \varrho \Phi \, dx \\ &= -\frac{1}{2\pi q^2} \int_{\mathbb{R}^3} \Phi \Delta_x \Phi \, dx = \frac{1}{2\pi q^2} \int_{\mathbb{R}^3} |\nabla_x \Phi|^2 \, dx \, , \end{aligned} \tag{81}$$

which we expect to be non-increasing along solutions of (79). Let us see how this behaviour is influenced by the additional diffusion in (80):

$$\begin{aligned} \frac{d}{dt} E^C[\varrho] &= \frac{1}{\pi q^2} \int_{\mathbb{R}^3} \nabla_x \Phi \cdot \partial_t \nabla_x \Phi \, dx = -\frac{1}{\pi q^2} \int_{\mathbb{R}^3} \Phi \, \partial_t \Delta_x \Phi \, dx \\ &= 2 \int_{\mathbb{R}^3} \Phi \, \partial_t \varrho \, dx = -\frac{2}{\kappa} \int_{\mathbb{R}^3} \nabla_x \Phi \cdot (D \nabla_x \varrho + \varrho \nabla_x \Phi) dx \\ &= -\frac{2}{\kappa} \int_{\mathbb{R}^3} \varrho |\nabla_x \Phi|^2 dx + \frac{2D}{\kappa} \int_{\mathbb{R}^3} \varrho \, \Delta_x \Phi \, dx \\ &= -\frac{2}{\kappa} \int_{\mathbb{R}^3} \varrho |\nabla_x \Phi|^2 dx - \frac{4\pi q^2 D}{\kappa} \int_{\mathbb{R}^3} \varrho^2 dx \leq 0 \, . \end{aligned}$$

The last term caused by diffusion actually makes the decay of the potential energy even faster. This should not be a surprise, since the Coulomb repulsion spreads the particles out, and diffusion does just the same. We expect that ϱ converges to zero locally.

An alternative approach to study the long-time behaviour is to look for steady states. It seems natural to request zero flux $D\nabla_x\varrho+\varrho\nabla_x\Phi = 0$ with the consequence

$$\varrho = \overline{\varrho}e^{-\Phi/D}\,, \tag{82}$$

with a constant of integration $\overline{\varrho} \geq 0$. Then the potential has to satisfy the nonlinear Poisson equation

$$\Delta_x\Phi = -2\pi q^2\overline{\varrho}e^{-\Phi/D}\,.$$

Without proof we state that for $\overline{\varrho} > 0$ this equation does not have a solution Φ such that $\varrho = \overline{\varrho}e^{-\Phi/D}$ is integrable, which means that there is no steady state with finite total charge. This statement is not necessarily true if, instead of the whole space $\mathbb{R}^3$, bounded domains are considered.

The digression should be taken as a motivation for our choice of the potential energy term describing Coulomb repulsion of parallel filaments. Actually we combine (81) with an equilibrium condition like (82) providing an explicit connection between the potential and the density:

$$\begin{aligned}\mathcal{E}^C(t)[F^\pm] &:= \int_{\mathcal{L}^\pm(t)} \Phi(\varrho^\pm)\varrho^\pm dx \\ &= \int_{B^\pm(t)} \Phi\left(\frac{\eta^\pm}{(\partial_\alpha F^\pm)^\perp\cdot\partial_s F^\pm}\right)\eta^\pm d(\alpha,s)\,,\end{aligned} \tag{83}$$

where we have used the connection (66) between the actin densities in Euler and, respectively, Lagrange coordinates.

Finally we consider forces acting at the ends of the filaments. Recalling from monk's sailboat (Section 5.2) that an external force is multiplied by the deviation to produce a contribution to the potential energy, the following should be plausible:

$$\mathcal{E}^f(t)[F^\pm] = -\int_{\mathbb{T}^1}\left(F^\pm(\alpha,0)\cdot f_0^\pm(\alpha,t) + F^\pm(\alpha,L^\pm)\cdot f_L^\pm(\alpha,t)\right)d\alpha\,, \tag{84}$$

where $f_0^\pm$ denotes the forces acting on the filament ends along the leading edge, and $f_L^\pm$ denotes the forces along the internal boundary of the lamellipodium. Usually the effect of these forces is to keep the cell together. There are two important mechanisms with this function. Membrane tension has already been described in Section 5.3. Here it would lead to a force along

the leading edge, i.e. at $s = 0$. On the other hand, there is a contractive structure in the internal part of the cell, which provides forces pulling at the pointed (interior) ends of the filaments, i.e. at $s = L^{\pm}$.

With the definitions (73), (75), (83), and (84), the total potential energy is now given by

$$\begin{aligned}\mathcal{E}^{pot}(t)[F^+,F^-] \;:=\; & \mathcal{E}^B(t)[F^+]+\mathcal{E}^B(t)[F^-]+\mathcal{E}^T(t)[F^+,F^-]+\mathcal{E}^C(t)[F^+] \\ & +\mathcal{E}^C(t)[F^-]+\mathcal{E}^f(t)[F^+]+\mathcal{E}^f(t)[F^-]\,. \qquad (85)\end{aligned}$$

Friction effects: We start with friction caused by adhesion between filaments and the substrate. The most important player is the transmembrane protein *integrin*, which can bind to extracellular material on the one hand and, via a complicated intracellular protein complex, to actin filaments on the other hand (see Fig. 25). For simplicity we shall assume that by this mechanism any point on an actin filament can be transiently connected to the substrate, resulting in friction between filament and substrate.

At this point we need to recall that, because of polymerization, s is not a Lagrange coordinate for the $\pm$-family, but $\sigma = s - \int_0^t v^{\pm}(\alpha,\tau)d\tau$ is (see (67)). This implies that a monomer, which has the coordinate s at time t, had the coordinate $s - \int_{t-h}^t v^{\pm}(\alpha,\tau)d\tau$ at time $t-h$. Therefore, if this monomer has been connected to the substrate at time $t-h$, it has been displaced by

$$F^{\pm}(\alpha,s,t) - F^{\pm}\left(\alpha, s - \int_{t-h}^t v^{\pm}(\alpha,\tau)d\tau, t-h\right),$$

and the connection has been stretched to the length of this displacement. This motivates the following adhesion stretching energy:

$$\begin{aligned}&\mathcal{E}^A(t,h)[F^{\pm}] \qquad (86)\\ &= \frac{\mu^A}{2h}\int_{B^{\pm}(t)}\left|F^{\pm} - F^{\pm}\left(\alpha, s - \int_{t-h}^t v^{\pm}(\alpha,\tau)d\tau, t-h\right)\right|^2 \eta^{\pm}d(\alpha,s)\,,\end{aligned}$$

with friction coefficient μ^A.

The second friction effect is between the filament families. It can be caused by breaking branches or by proteins like *filamin* (see Fig. 26). We are now interested in a displacement

$$F^+(\alpha^+,s^+,t) - F^-(\alpha^-,s^-,t)\,,$$

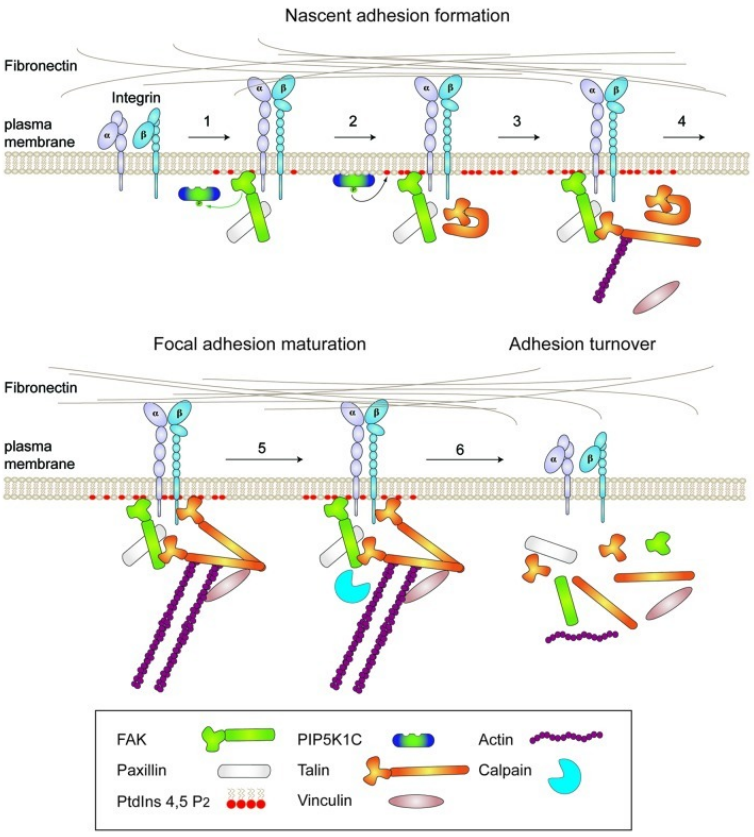

Figure 25: Dynamics of adhesion complexes. Source: [7].

where the two monomers have been at the same place and have been connected there at time $t-h$. With the notation for crossing filaments introduced in (74) and with the approximation $\int_{t-h}^{t} v^{\pm} \approx h v^{\pm}$, this implies

$$\begin{aligned} & s^{\pm} - h v^{\pm} = S^{\pm}(\alpha^{+}, \alpha^{-}, t-h) \qquad \Leftrightarrow \\ & F^{+}(\alpha^{+}, s^{+} - h v^{+}, t-h) = F^{-}(\alpha^{-}, s^{-} - h v^{-}, t-h)\,, \end{aligned} \tag{87}$$

and the above displacement can be written as

$$F^{+}(\alpha^{+}, S^{+} + h v^{+}, t) - F^{-}(\alpha^{-}, S^{-} + h v^{-}, t)\,.$$

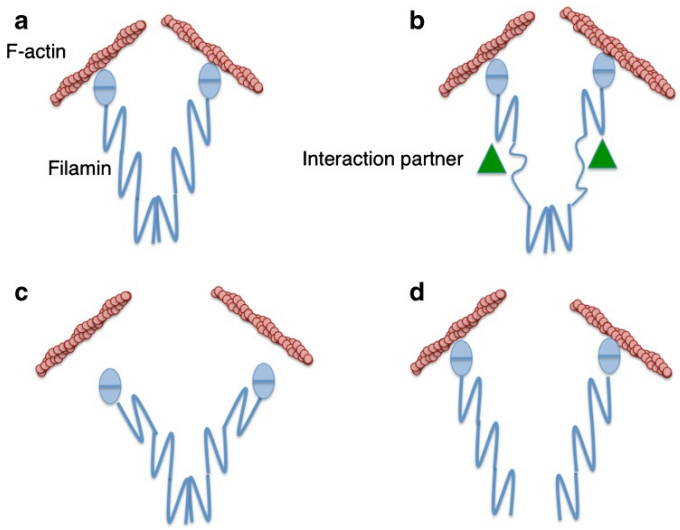

Figure 26: Actin filament cross-linking by filamin, which may react to stress by (b) partial unfolding, (c) detachment from actin, (d) breaking its dimeric structure. Source: [19].

Now it is straightforward to write a stretching energy for cross-links:

$$\begin{aligned}&\mathcal{E}^S(t,h)[F^+,F^-] \qquad (88)\\ &= \frac{\mu^S}{2h}\int_{A_C(t-h)} \left|F^+(\alpha^+,S^+ + hv^+,t) - F^-(\alpha^-,S^- + hv^-,t)\right|^2 \eta^+\eta^- d(\alpha^+,\alpha^-)\,,\end{aligned}$$

with $\eta^\pm = \eta^\pm(\alpha^\pm, S^\pm, t-h)$. Note however that the assumption that the energy goes with the square of the displacement length is questionable. If one considers Fig. 26 **b** for example, showing that stretching of filamin involves partial unfolding, it can be expected that the correct potential energy is more complicated in this situation.

We combine the stretching energies into

$$\mathcal{E}^{friction}(t,h)[F^+,F^-] := \mathcal{E}^A(t,h)[F^+] + \mathcal{E}^A(t,h)[F^-] + \mathcal{E}^S(t,h)[F^+,F^-]\,. \quad (89)$$

Putting everything together: Now we are ready to formulate the complete model. We recall the constraints (64), (65) by defining

$$\begin{aligned}\mathcal{F}(t) \;=\; \big\{(F^+,F^-)\;\big|\; &F^\pm : B^\pm(t)\to\mathbb{R}^2\,,\ |\partial_s F^\pm| = 1\,, \qquad (90)\\ &\{F^+(s=0)\} = \{F^-(s=0)\}\big\}\,. \qquad (91)\end{aligned}$$

Then the *Filament Based Lamellipodium Model* is completed by

$$
\begin{aligned}
&(F^+(\cdot,\cdot,t), F^-(\cdot,\cdot,t)) \qquad (92)\\
&= \lim_{h\to 0} \operatorname*{argmin}_{(G^+,G^-)\in\mathcal{F}(t)} \left(\mathcal{E}^{friction}(t,h)[G^+,G^-] + \mathcal{E}^{pot}(t)[G^+,G^-]\right) .
\end{aligned}
$$

recalling (85), (89). It determines (F^+, F^-) for given (η^+, η^-) which in turn is the solution of (70)–(72).

The next step is the derivation of a formulation in terms of differential equations. This requires the definition of a Lagrangian functional by taking into account the constraints in (90). This has been carried out for the arclength constraint in Section 5.7. The second constraint, which involves an equality between sets needs to be rewritten as a system of local equations. The details will be omitted here. Unconstrained stationary points of the Lagrangian have to satisfy the Euler-Lagrange equations we are looking for. This requires to compute gradients of all the energy terms in (85) and (89). We shall present only two examples, one contribution to the potential energy and one friction contribution.

The first example is the Coulomb repulsion term (83), which we rewrite without superscripts and without the time argument for simplicity:

$$
\mathcal{E}^C[F] = \int_B \Phi\left(\varrho\right) \eta \, d(\alpha, s) \,, \qquad \text{with } \varrho = \varrho[F] = \frac{\eta}{\partial_\alpha F^\perp \cdot \partial_s F} \,.
$$

As a preparation we compute

$$
\varrho[F+\delta G] = \frac{\eta}{(\partial_\alpha F^\perp + \delta \partial_\alpha G^\perp)\cdot(\partial_s F + \delta \partial_s G)} \,,
$$

and

$$
\frac{d}{d\delta}\varrho[F+\delta G]\,\big|_{\delta=0} = \frac{-\eta}{(\partial_\alpha F^\perp \cdot \partial_s F)^2}(\partial_\alpha F^\perp \cdot \partial_s G - \partial_s F^\perp \cdot \partial_\alpha G) \,,
$$

where we have used $a^\perp \cdot b = a^{\perp\perp}\cdot b^\perp = -a\cdot b^\perp$. With the *pressure* $p(\varrho) := \Phi'(\varrho)\varrho^2$ this implies

$$
\begin{aligned}
\frac{d}{d\delta}\mathcal{E}^C[F+\delta G]\,\big|_{\delta=0} &= \int_B p(\varrho)(\partial_s F^\perp \cdot \partial_\alpha G - \partial_\alpha F^\perp \cdot \partial_s G) d(\alpha,s)\\
&= \int_B (\partial_s(p(\varrho)\partial_\alpha F^\perp) - \partial_\alpha(p(\varrho)\partial_s F^\perp))\cdot G \, d(\alpha,s)\\
&\quad - \int_{\mathbb{T}^1} p(\varrho)\partial_\alpha F^\perp \cdot G\,\big|_{s=0}^{L}\, d\alpha \,.
\end{aligned}
$$

Similarly to the computation for the bending energy (see Section 5.7), the first term on the right hand side will contribute to the differential equations and the second to the boundary conditions. Note that by periodicity the integration by parts with respect to α does not produce any boundary terms.

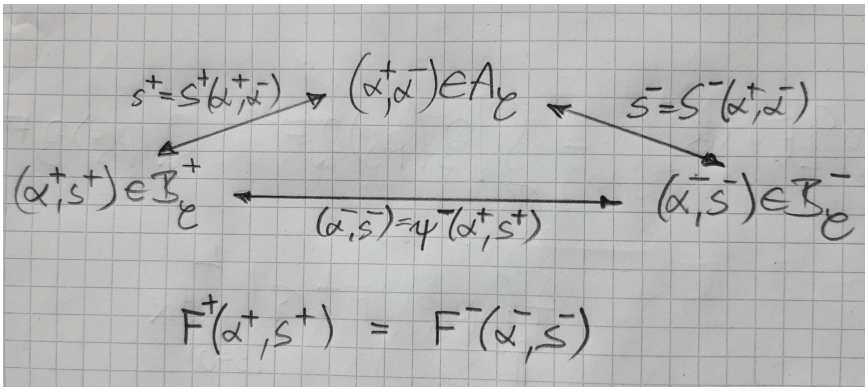

Figure 27: Coordinate transformations for crossing filaments.

Now we consider the stretching energy of cross-links (88) and compute its gradient with respect to F^+. We start with

$$\mathcal{E}^S(t,h)[F^+ + \delta G^+, F^-] = \frac{\mu^S}{2h} \int_{A_C(t-h)} \big| F^+(\alpha^+, S^+ + hv^+, t) + \delta G^+(\alpha^+, S^+ + hv^+, t) - F^-(\alpha^-, S^- + hv^-, t) \big|^2 \eta^+ \eta^- d(\alpha^+, \alpha^-)\,,$$

and

$$\frac{d}{d\delta} \mathcal{E}^S(t,h)[F^+ + \delta G^+, F^-]\,\big|_{\delta=0} = \frac{\mu^S}{h} \int_{A_C(t-h)} \big(F^+(\alpha^+, S^+ + hv^+, t) - F^-(\alpha^-, S^- + hv^-, t) \big) \cdot G^+(\alpha^+, S^+ + hv^+, t) \eta^+ \eta^- d(\alpha^+, \alpha^-)\,.$$

The next step is the limit $h \to 0$. Recalling (87), i.e. $F^+(\alpha^+, S^+, t-h) =$

$F^-(\alpha^-, S^-, t-h)$, we have

$$\begin{aligned}
&\frac{1}{h}\left(F^+(\alpha^+, S^+ + hv^+, t) - F^-(\alpha^-, S^- + hv^-, t)\right) \\
&= \frac{F^+(\alpha^+, S^+ + hv^+, t) - F^+(\alpha^+, S^+, t-h)}{h} \\
&\quad + \frac{F^-(\alpha^-, S^-, t-h) - F^-(\alpha^-, S^- + hv^-, t)}{h} \\
&\underset{h\to 0}{\to} \quad D_t^+ F^+(\alpha^+, S^+, t) - D_t^- F^-(\alpha^-, S^-, t)\,,
\end{aligned}$$

using the definition (68) of the material derivatives: $D_t^\pm = \partial_t + v^\pm \partial_s$. This result is no surprise. It is just the relative velocity between monomers on crossing filaments. We obtain

$$\begin{aligned}
&\lim_{h\to 0} \frac{d}{d\delta} \mathcal{E}^S(t,h)[F^+ + \delta G^+, F^-]\,\big|_{\delta=0} \\
&= \mu^S \int_{A_\mathcal{C}(t)} \left(D_t^+ F^+(\alpha^+, S^+, t) - D_t^- F^-(\alpha^-, S^-, t)\right) \cdot G^+(\alpha^+, S^+, t)\eta^+\eta^- d(\alpha^+, \alpha^-)\,,
\end{aligned}$$

In order to get a result which can be combined with the Coulomb interaction, we need a transformation to the same domain. For this purpose the coordinate transformations for crossing filaments are recalled in Fig. 27. We transform $A_\mathcal{C}(t)$ to $B_\mathcal{C}^+(t)$ by $(\alpha, s) = (\alpha^+, S^+(\alpha^+, \alpha^-, t))$, where we introduce the inverse as $(\alpha^+, \alpha^-) = (\alpha, A^-(\alpha, s, t)$. Note that for the argument of F^- this gives $(\alpha^-, S^-(\alpha^+, \alpha^-, t)) = \psi^-(\alpha, s, t)$. This leads to the final result

$$\begin{aligned}
&\lim_{h\to 0} \frac{d}{d\delta} \mathcal{E}^S(t,h)[F^+ + \delta G^+, F^-]\,\big|_{\delta=0} \\
&= \int_{B^+(t)} \widehat{\mu}^S \left(D_t^+ F^+ - D_t^- F^- \circ \psi^-\right) \cdot G^+ \eta^+ (\eta^- \circ \psi^-) d(\alpha, s)\,,
\end{aligned}$$

with

$$\widehat{\mu}^{S,+} = \mu^S \mathbb{1}_{B_\mathcal{C}^+(t)} \left|\partial_s A^-\right|\,.$$

Proceeding similarly with all the other terms in the Lagrangian leads to the Euler-Lagrange equations

$$\begin{aligned}
0 \;=\; & \mu^B \partial_s^2(\eta^\pm \partial_s^2 F^\pm) - \partial_s(\eta^\pm \lambda^\pm \partial_s F^\pm) + \mu^A \eta^\pm D_t^\pm F^\pm \\
& + \partial_s(p(\varrho^\pm)(\partial_\alpha F^\pm)^\perp) - \partial_\alpha(p(\varrho^\pm)(\partial_s F^\pm)^\perp) \\
& \pm \partial_s(\widehat{\mu}^{T,\pm} \eta^\pm (\eta^\mp \circ \psi^\mp)(\varphi - \varphi_0)(\partial_s F^\pm)^\perp) \\
& + \widehat{\mu}^{S,\pm} \eta^\pm (\eta^\mp \circ \psi^\mp)(D_t^\pm F^\pm - D_t^\mp F^\mp \circ \psi^\mp)\,,
\end{aligned}$$

subject to the boundary conditions

$$
\begin{aligned}
&\partial_s^2 F^{\pm} = 0 \qquad \text{for } s = 0, L^{\pm}\,, \\
&-\mu^B \partial_s(\eta^{\pm}\partial_s^2 F^{\pm}) + \eta^{\pm}\lambda^{\pm}\partial_s F^{\pm} - p(\varrho^{\pm})(\partial_\alpha F^{\pm})^{\perp} \\
&\quad \mp \widehat{\mu}^{T,\pm}\eta^{\pm}(\eta^{\mp}\circ\psi^{\mp})(\varphi-\varphi_0)(\partial_s F^{\pm})^{\perp} = -f_0^{\pm} \pm \lambda_{tether}\nu \qquad \text{for } s = 0\,, \\
&-\mu^B \partial_s(\eta^{\pm}\partial_s^2 F^{\pm}) + \eta^{\pm}\lambda^{\pm}\partial_s F^{\pm} - p(\varrho^{\pm})(\partial_\alpha F^{\pm})^{\perp} \\
&\quad \mp \widehat{\mu}^{T,\pm}\eta^{\pm}(\eta^{\mp}\circ\psi^{\mp})(\varphi-\varphi_0)(\partial_s F^{\pm})^{\perp} = f_L^{\pm} \qquad \text{for } s = L^{\pm}\,,
\end{aligned}
$$

where $\widehat{\mu}^{T,\pm}$ is defined analogously to $\widehat{\mu}^{S,\pm}$, $\nu = (\partial_\alpha F^{\pm})^{\perp}/|\partial_\alpha F^{\pm}|$ is the normalized normal vector along the leading edge, and λ_{tether} is the Lagrange multiplier for the leading edge constraint. The explanation for the subscript *tether* is that the leading edge constraint can be motivated by the assumption that the barbed ends of the filaments are tethered to the membrane at the leading edge. This produces a pulling (outward) force on the family, which would fall behind without the constraint, and a pushing (inward) force of equal size on the other family.

5.9 Simulations with the FBLM

To write a simulation program on the basis of the FBLM is a formidable enterprise, which will not be discussed here (but see [9]). However, part of the potential of the FBLM will be demonstrated in this section by showing simulation results. We begin with cell movement influenced by chemotactic signals and consider a given chemotactic signal in the form of a gradient of a chemoattractant. This is translated to an internal signal for the filament production machinery along the leading edge. Fig. 29 shows snapshots of a simulation starting with a circular shaped cell receiving a chemotactic signal from the right, leading to a polymerization speed, which is gradually increased towards the right. The cell deforms, develops a wider lamellipodium on the right, and starts to move.

The simulation illustrated in Fig. 30 starts with the final state of the preceding simulation, and then the direction of the chemotactic signal is gradually turned by 45^o. The figure shows the evolution of the leading edge.

Depending on the internal transmission of the chemotactic signal, different moving cell shapes are observed. Actually there is evidence that cells tend to internally concentrate the signal received from outside. In Fig. 31 shapes of moving cells are shown for different concentrations of the chemotactic signal and also for the case where the signal increases not the polymerization speed, but the branching rate. In this case not a wider, but a denser lamellipodium is observed.

In experiments it is possible to produce substrates with locally variable adhesiveness, i.e. integrin binding properties. In the FBLM this is translated to a locally varying friction coefficient $\mu^A = \mu^A(F^{\pm})$. Figs. 32 and 33 show snapshots of simulations of cells moving under the influence of a chemotactic signal on substrates with variable adhesiveness.

Since the parts of the FBLM corresponding to various molecular effects are clearly separated, it is easy to remove or add effects. An example is the interaction between actin and *myosin* filaments, which is also the basic effect in muscle contraction. Myosin is a *motor protein* which binds to actin and, by conformation changes, is able to move along actin filaments. It also occurs in polymerized form as filaments with two parts with opposite orientation. If both parts bind to actin filaments, the motor behaviour leads to contraction of the actin filaments. In muscles, actin filaments occur in organized bundles, but in our cells we attribute to myosin also a bundling activity, by turning actin filaments towards an anti-parallel state (see Fig. 28). In the FBLM, the myosin effect results in an additional term similar to cross-link stretching, which acts only, if the two families are anti-parallel enough, which has a turning effect with equilibrium angle $\varphi_0 = \pi$, and which has an account of the motor activity. Fig. 34 shows snapshots of two simulations with a small difference between the initial conditions, showing bistable behaviour of the cell. In one case it tends to a circular nonmoving state, and in the other case to a polarized moving state. Note that in these experiments there is no chemotactic signal.

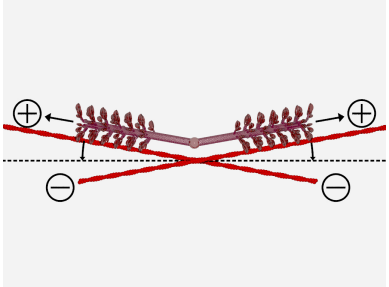

Figure 28: A myosin filament acting on a pair of actin filaments with roughly opposite orientation. Source: [6].

Another extension deals with the interaction between cells. This involves so called *steric repulsion*, avoiding overlap between cells, but potentially also *cell-cell adhesion*. Fig. 35 shows a snapshot of a simulation of a cell ensemble taking into account cell-cell adhesion, a chemotactic signal, and

variable substrate adhesion.

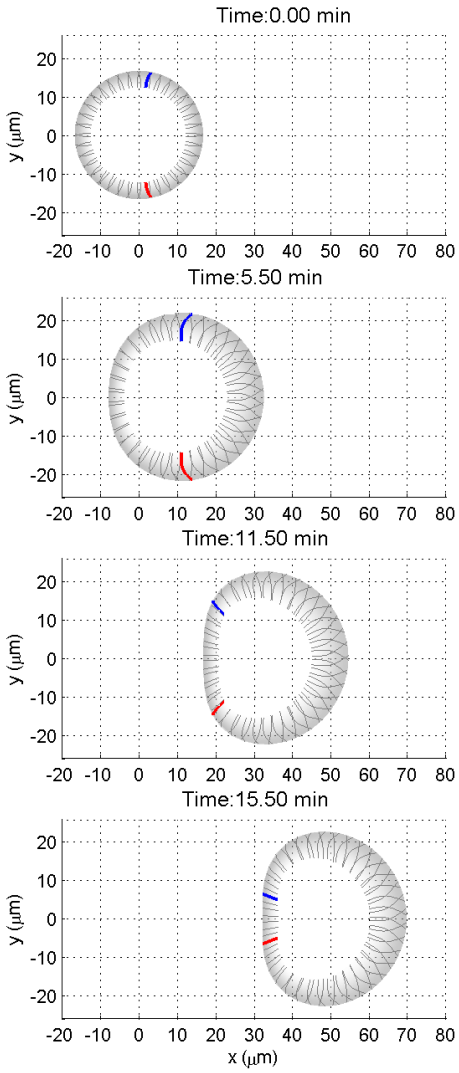

Figure 29: Time series of a cell under the influence of a chemotactic signal, starting with a rotationally symmetric shape. Source: [8].

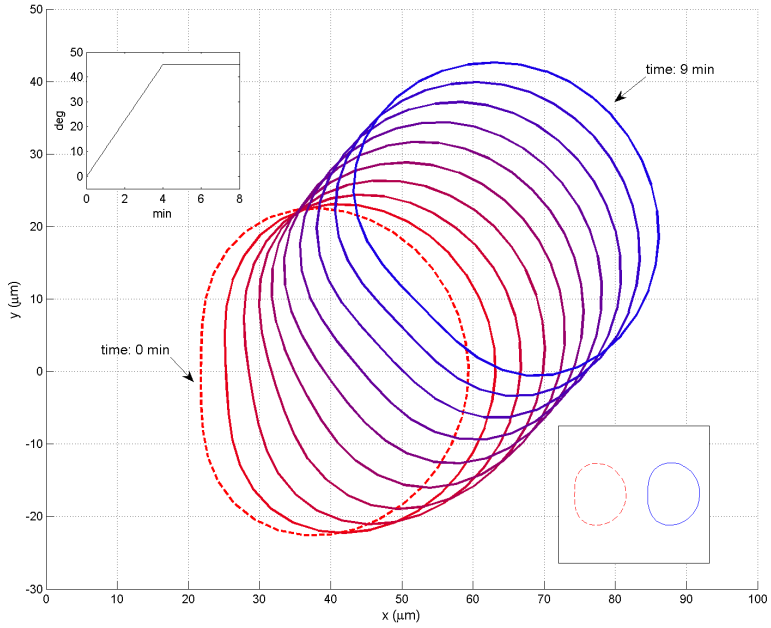

Figure 30: Time series of the leading edge of a cell under the influence of a turning chemotactic signal. The inserts show the prescribed evolution of the signal direction and a comparison of the cell shapes before and after the turning process. Source: [8].

References

[1] G. Bernot, J.-P. Comet, A. Richard, M. Chaves, J.-L. Gouze, F. Dayan, Modeling and analysis of gene regulatory networks, in *Modeling in Computational Biology and Biomedicine, A Multidisciplinary Endeavor* (eds. F. Cazals and P. Kornprobst). pp. 47-80, Springer, 2013.

[2] E. Bianconi et al., An estimation of the number of cells in the human body, *Ann. Hum. Biol.* 40(6) (2013), pp. 463–471.

[3] L.C. Evans, *Partial Differential Equations*, Graduate Studies in Mathematics 19, AMS, Providence, 1998.

[4] K. Fellner, W. Prager, B.Q. Tang, The entropy method for reaction-diffusion systems without detailed balance: first order chemical reaction networks, *arXiv:* 1504.08221

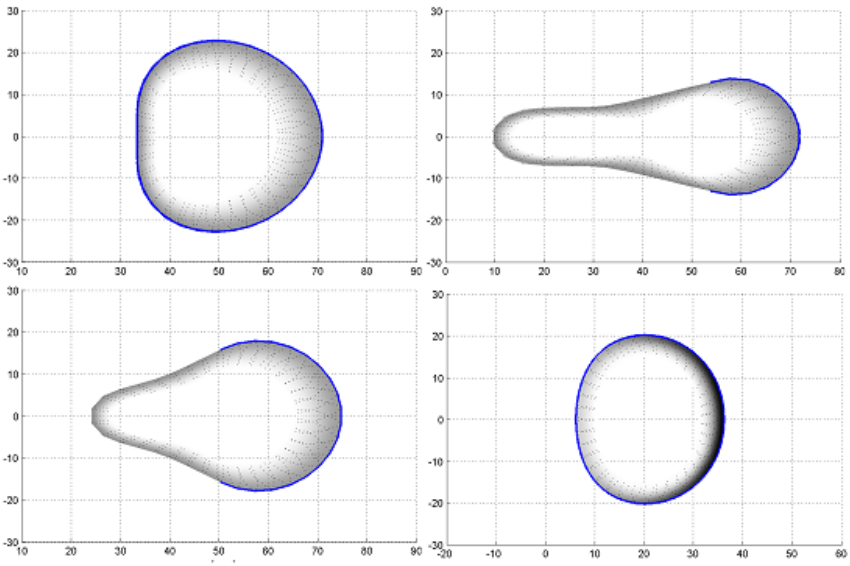

Figure 31: Different moving cell shapes. The blue part of the leading edge shows where the internal chemotactic signal is active. Top left, bottom left, and top right: more and more concentrated signal increasing the polymerization speed. Bottom right: internal signal increasing the branching rate. Source: [8].

[5] A.F. Filippov, Differential equations with discontinuous right hand side, *AMS Transl.* 42 (1962), pp. 199–231.

[6] S. Hirsch, A. Manhart, C. Schmeiser, Mathematical modeling of myosin induced bistability of lamellipodial fragments, *J. Math. Biol.* 74 (2017), pp. 1–22.

[7] C. Lawson, D.D. Schlaepfer, Integrin adhesions. Who's on first? What's on second?, *Cell Adhesion & Migration* 6 (2012), pp. 302–306.

[8] A. Manhart, D. Oelz, C. Schmeiser, N. Sfakianakis, An extended Filament Based Lamellipodium Model produces various moving cell shapes in the presence of chemotactic signals, *J. Theor. Biol.* 382 (2015), pp. 244–258.

[9] A. Manhart, D. Oelz, C. Schmeiser, N. Sfakianakis, Numerical treatment of the Filament Based Lamellipodium Model, in *Modeling Cellular Systems*, eds. F. Graw, F. Matthus, and J. Pahle, Springer, 2017.

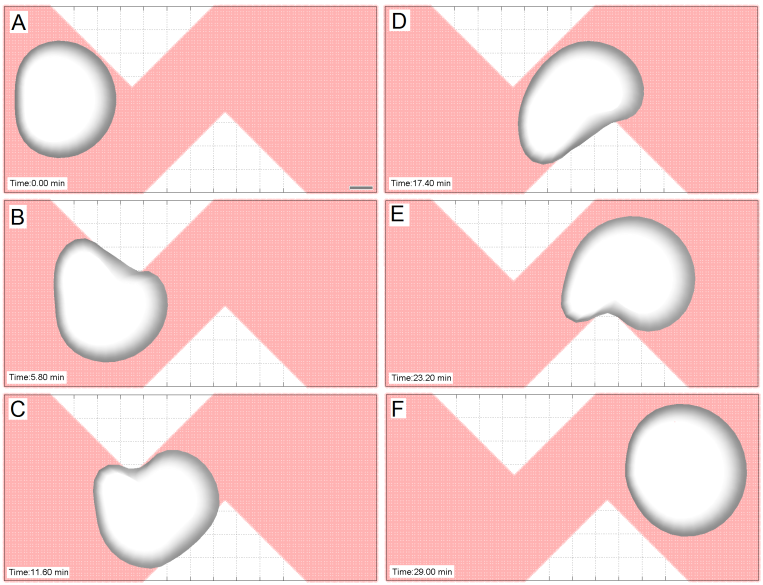

Figure 32: Time series of a cell moving under the influence of a chemotactic signal on a substrate with variable adhesiveness. High adhesiveness in pink, low adhesiveness in white. Source: [9].

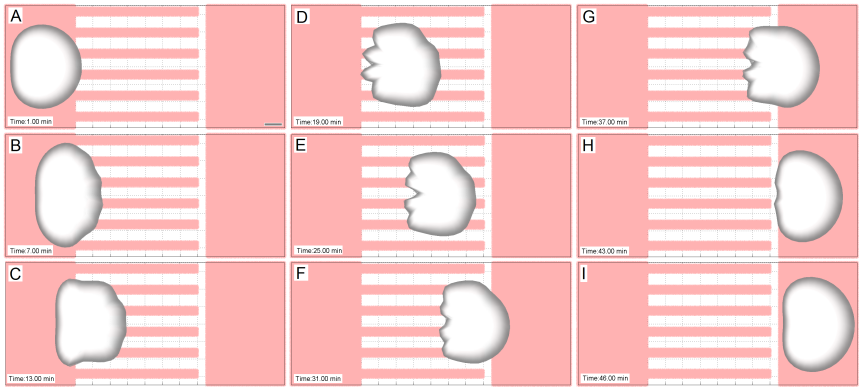

Figure 33: Time series of a cell moving under the influence of a chemotactic signal on a substrate with variable adhesiveness. High adhesiveness in pink, low adhesiveness in white. Source: [9].

[10] A. Manhart, C. Schmeiser, Existence of and decay to equilibrium of the filament end density along the leading edge of the lamellipodium,

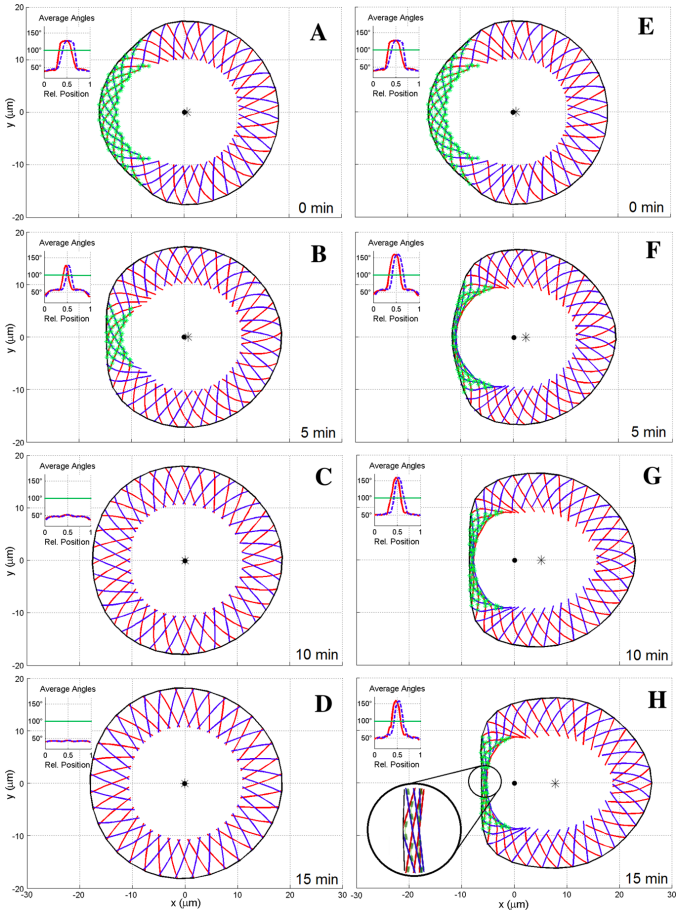

Figure 34: Two simulations incorporating actin-myosin interaction (green) and with slightly different initial configurations. Source: [6].

J. Math. Biol. 74 (2017), pp. 169–193.

[11] L. Michaelis, M. L. Menten, Die Kinetik der Invertinwirkung, *Biochem. Z.* 49 (1913), pp. 333-369.

[12] V. Milisic, D. Oelz, *J. Math. Pures Appl.* 96 (2011), pp. 484–501.

[13] D. Oelz, On the curve straightening flow of inextensible, open, planar curves, *SeMA Journal* 54 (2011), pp. 5–24.

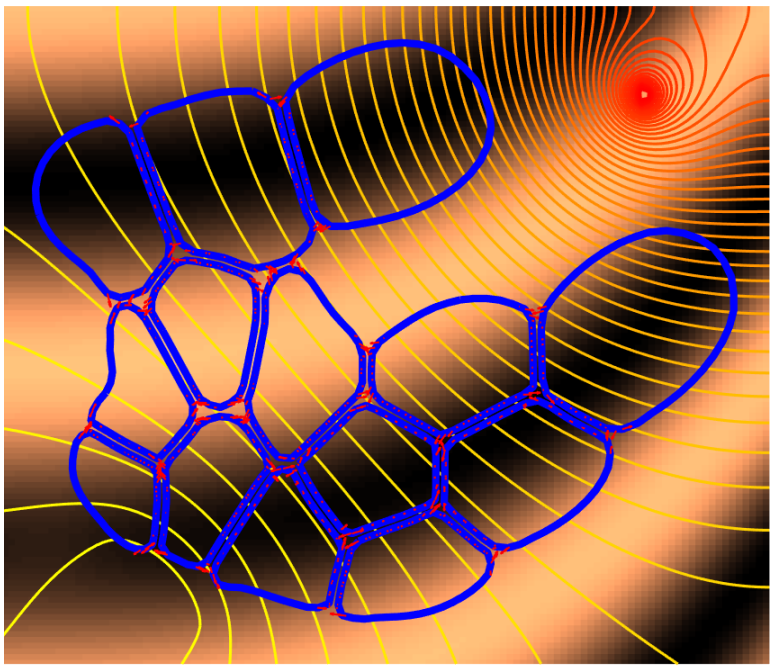

Figure 35: Snapshot of the simulation of a cell ensemble with cell-cell adhesion (red arrows), chemotaxis (yellow level lines of the chemoattractant density), and variable substrate adhesion (background shading). Source: [18].

[14] K. Parmar, K.B. Blyuss, Y.N. Kyrychko, S.J. Hogan, Time-delayed models of gene regulatory networks, *Comp. and Math. Meth. in Medicine* 2015 (2015), Article ID 347273.

[15] Q.-C. Pham, A variation of Gronwall′s lemma, *arXiv:* 0704.0922v3.

[16] M. Santillan, On the use of the Hill functions in mathematical models of gene regulatory networks, *Mathematical Modelling of Natural Phenomena* 3 (2008), pp. 85–97.

[17] T. Scheper, D. Klinkenberg, C. Pennartz, J. v. Pelt, A mathematical model for the intracellular circadian rhythm generator, *J. of Neurosci.*

19 (1999), pp. 40–47.

[18] N. Sfakianakis, D. Peurichard, A. Brunk, C. Schmeiser, Modelling cell-cell collision and adhesion with the Filament Based Lamellipodium Model, *Biomath* 7 (2018), Article ID: 1811097.

[19] A.J. Sutherland-Smith, Filamin structure, function and mechanics: are altered filamin-mediated force responses associated with human disease? *Biophys Rev.* 3 (2011), pp. 15–23.

[20] M. Vinzenz, M. Nemethova, F. Schur, J. Mueller, A. Narita, E. Urban, C. Winkler, C. Schmeiser, S. Koestler, K. Rottner, G.P. Resch, Y. Maeda, J.V. Small, Actin branching in the initiation and maintenance of lamellipodia, *J. Cell Sci.* 125 (2012), pp. 2775–2785.